

Compositional variations in deep-sea gravity-flow deposits. A case study from the Voirons Flysch (Voirons-Wägital complex, Chablais Prealps, France)

Jérémie Ragusa ^{*}, Pascal Kindler

Department of Earth Sciences, University of Geneva, Rue des Maraîchers 13, 1205 Geneva, Switzerland

ARTICLE INFO

Article history:

Received 26 June 2018

Received in revised form 23 August 2018

Accepted 24 August 2018

Available online 30 August 2018

Editor: Dr. B. Jones

Keywords:

Prealps

Flysch

Grain-size

Turbidite

Provenance analysis

Contourite

ABSTRACT

Grain-size control is frequently invoked to explain the compositional variation of detrital sediments in fluvial sediments. A similar possibility is here investigated in the fossil deep-sea gravity-flow deposits from the Voirons Flysch (Voirons-Wägital complex, Chablais Prealps). About 270 samples of diverse depositional settings were analysed using the framework composition, including cement and porosity, Mutti facies and grain-size measurements. Six lithofacies have been identified from cluster analysis. They correspond to channel (L1 to L3) and lobe (L4 and L5) depositional settings and to reworked turbidites (L6). Our results emphasize the close relationship between petrography and grain-size which alters the detrital signal from extrabasinal sources. The abundant polycrystalline component of proximal deposits is progressively removed while skeletal grains and additional intrabasinal grains become more abundant in distal deposits. Alongside, porosity is reduced by the simultaneous increase of cement which constrains subsequent diagenetic modifications. Hence, proximal depositional settings keep most of the inherited signal from extrabasinal sources whereas distal deposits will be homogenised. When plotted in provenance-analysis diagrams, the successive depositional settings show distinct fields possibly corresponding to different tectonic settings of the Dickinson model. This compositional variation thus creates a bias in provenance interpretation resulting from both grain-size control and flow mechanisms. Finally, our results emphasize that petrographic data must be handled with care in provenance analyses, especially when comparing various deep-sea gravity flow systems with different grain-size ranges.

© 2018 Elsevier B.V. All rights reserved.

1. Introduction

The mineralogical composition of detrital sediments is primarily controlled by the tectonic setting during deposition (Krynine, 1943; Dickinson, 1974; Suttner, 1974; Folk, 1980), which determines rock exposures in the catchment area, and by the duration and intensity of weathering processes (Suttner et al., 1981; Johnsson, 1993; Amorosi and Zuffa, 2011). The tectonic setting of the source areas can be inferred by plotting the detrital composition of the investigated sediments in the ternary diagrams of the Dickinson model (Dickinson and Suczek, 1979; Dickinson, 1985) or of the most recent Garzanti model (Garzanti et al., 2007) using the Gazzi-Dickinson method (Gazzi, 1966; Gazzi et al., 1973; Dickinson, 1974). The Gazzi-Dickinson method is believed to reduce the grain-size dependence (Dickinson and Suczek, 1979; Ingersoll et al., 1984), which is nonetheless only partly removed (Decker and Helmold, 1985; Ingersoll et al., 1985a, 1985b; Suttner and Basu, 1985; Zuffa, 1985, 1987), as different modal composition can be observed in the same sediment from different grain-size ranges (Basu,

1976; Garzanti et al., 2008). Thus, the nature of coarse-grained lithic fragments depends on the sand grain-size (Zuffa, 1985, references herein). Similarly, mechanical breakdown of feldspars along cleavage improves their preservation in fine-grained sediments (Odom, 1975; Garzanti, 1986) which retain an arkosic composition in siltstone and mudstone (for example Bloch et al., 2006). Furthermore, these sediments provide a preferential lower weathering rate than equivalent sandstones (Milliken, 1992). Grain-size fractionation results from (1) the mechanical breakdown of polymineralic grains (e.g. rock fragments) and (2) the chemical and physical properties of each mineral species (density, shape and cleavage). The latter determine their preservation potential within each grain-size range (Morton and Hallsworth, 1999). Mineralogical properties also control the settling of each grain which can be understood with the *hydraulic equivalence* (Rubey, 1933) and its derivative the *settling equivalence* (Burroughs, 1985; Komar, 2007; Garzanti et al., 2008, 2009). The concept of hydraulic equivalence postulates the simultaneous deposition of grains having the same settling velocity and hence, explains the occurrence of fine-grained heavy minerals within coarse sediments. Thus, recent studies in fluvial and beach sediments emphasised a compositional variation of the major framework grains (Misko and Hendry, 1979; Suttner

* Corresponding author.

E-mail address: jeremy.ragusa@hotmail.fr (J. Ragusa).

et al., 1981; Garzanti, 1986; Grantham and Velbel, 1988; Johnsson, 1993; Kairo et al., 1993) and heavy minerals (Trask and Hand, 1985; Tomkins et al., 2003; Komar, 2007; Garzanti et al., 2008, 2009; Pyles et al., 2013; Garzanti et al., 2015) throughout the grain-size distribution.

Gravity-flow deposits are prime candidates to investigate these questions because they are characterised by downstream flow transformation and a fining-upward grain-size gradient (Stow and Shanmugam, 1980; Lowe, 1982; Mutti, 1992; Mulder and Alexander, 2001). The sedimentary architecture (Kuenen and Migliorini, 1950; Bouma, 1962; Mutti, 1972; Walker, 1973; Ricci-Lucchi, 1975; Lowe, 1982; Postma et al., 2009; Cartigny et al., 2014) and the grain-size variation (Sestini, 1970; Komar, 1985; Gladstone and Sparks, 2002; Weltje and Prins, 2003; Stevenson et al., 2014) of sediment gravity flows have been largely examined, but only a few studies addressed the relationship of the basinward evolution and grain-size fining trend with petrography (Stanley, 1963; Norman, 1969; Shideler et al., 1975; Korsch et al., 1993; Dutton and Loucks, 2010; Pyles et al., 2013) or geochemistry (McLennan et al., 1989; Korsch et al., 1993; Kiminami and Fujii, 2007; Cantalejo and Pickering, 2014). The recent provenance analysis of the Voiron Flysch (Ragusa, 2015; Ragusa et al., 2017) thus represents a unique opportunity to observe a large variety of sedimentary fabrics in deep-sea gravity-flows deposits from proximal to distal settings. Herein, the framework composition is compared to the grain-size distribution and the sedimentary features throughout the study of

several lithofacies. A depositional model is proposed as well as a brief description of the subsequent diagenetic processes. Finally, the relative location of the lithofacies within the depositional system and the grain-size are compared in the framework of the provenance analysis and their implications discussed.

2. Geological setting

The Alps result from the convergence of the European and the African plates, and the subsequent closure of the Alpine Tethys during Cretaceous-Palaeogene times (Schmid et al., 1996; Handy et al., 2010). The mountain chain comprises several low-elevation reliefs, such as the Chablais massif (or Chablais Prealps), which is located to the south of Lake Geneva, straddling France and Switzerland (Fig. 1). This massif belongs to the former accretionary prism of the Western to Central Alps and consists of a stack of sedimentary cover nappes (Caron, 1973; Caron et al., 1989) (Fig. 1) including, in ascending order, units originating from the European margin (Ultrahelvetic realm), the Valais Ocean, the Briançonnais micro-continent and the Piemont Ocean. These nappes were detached from their basement during the subduction of the Alpine Tethys, following a thin-skinned, in-sequence thrusting (Mosar, 1991; Wissing and Pfiffner, 2002). Nowadays, the Chablais massif overlies the Helvetic nappes to the SE and the North Alpine Foreland Basin to the NW (Fig. 1).

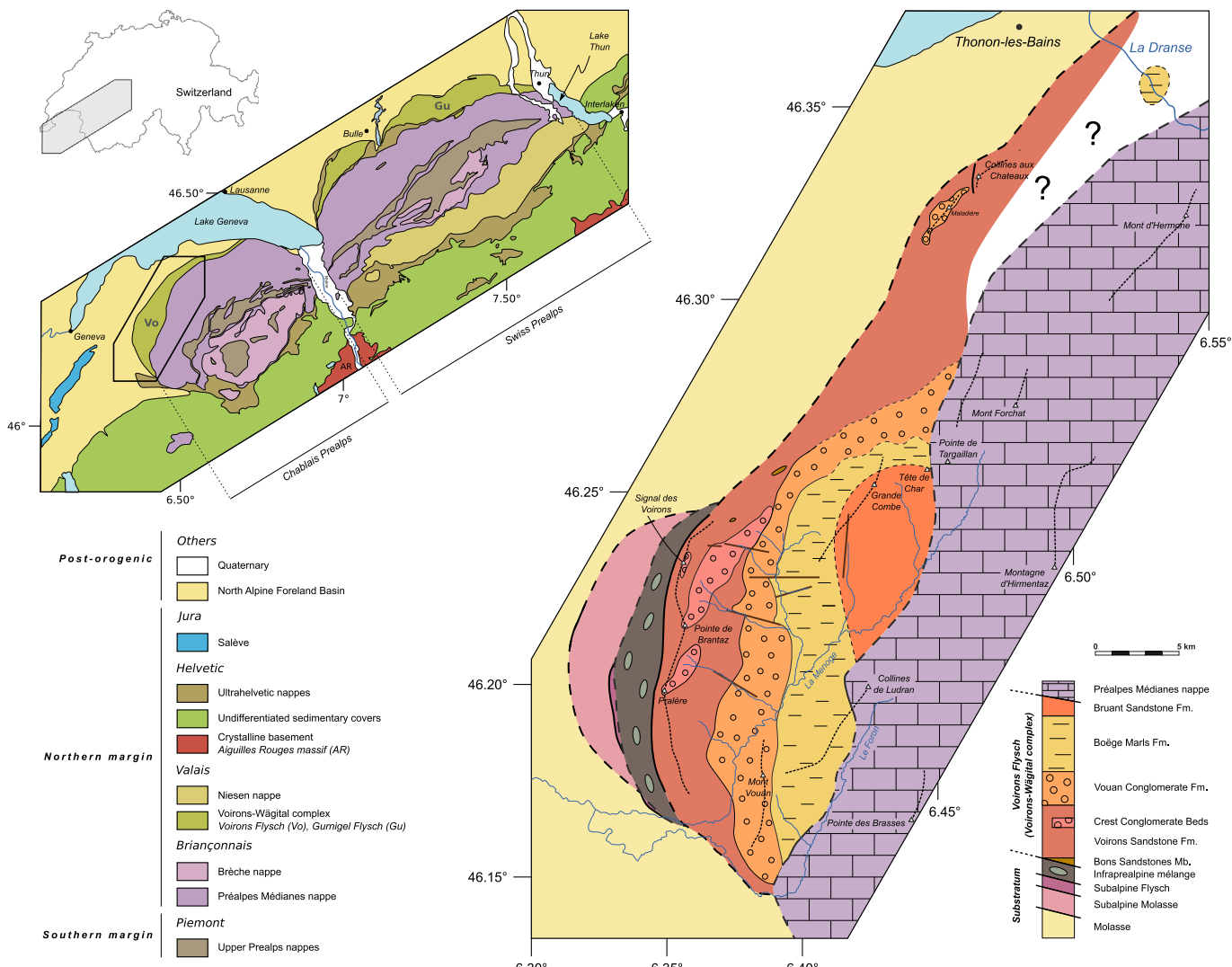


Fig. 1. Geological settings of the Voiron Flysch. (left) Tectonic map of the Chablais and Swiss Prealps (SwissTopo, 2008, modified) with the location of the Voiron and Gurnigel Flyschs of the Voiron-Wägital complex. (right) Geological map of the Voiron Flysch (Ragusa et al., 2017, modified).

Located along the outer edge of the Chablais massif, the Voirons-Wägital complex, formerly called Gurnigel nappe (Caron, 1976), is one of the lowermost Prealpine units (Fig. 1). This unit extends throughout the Swiss Prealps to Lake Zurich to the NE. It corresponds to a detrital accumulation generally interpreted as deep-sea gravity-flow deposits (i.e. a flysch; Kuenen and Carozzi, 1953; Frébourg, 2006) based on the *Rhabdamina* fauna found in some marly intervals (Brouwnier, 1965; Weidmann, 1967; Van Stuijvenberg et al., 1976; Ujetz, 1996) and the ichnofacies associations (Crimes et al., 1981). Recurrent plant fragments observed on top of many beds suggest deposition by extrabasinal gravity flows (e.g. hyperpycnal flows; Zavala and Arcuri, 2016). Detrital sediments originate from the southern margin of the Alpine Tethys (Winkler, 1984; Caron et al., 1989; Bütlér et al., 2011). However, the exact palaeogeographic location of the Voirons-Wägital complex remains controversial and is placed either in the Piemont domain (Caron, 1972; Caron et al., 1980; Winkler, 1983, 1984; Bütlér et al., 2011) or in the Valais realm (Ujetz, 1996; Trümpy, 2006; Ospina-Ostios et al., 2013; Ragusa et al., 2017; Ragusa et al., 2018) considering, respectively, calcareous-nannofossil assemblages (Maastrichtian – Middle Eocene) and planktonic-foraminifera associations (Early to Late Eocene).

The Voirons Flysch represents the westernmost flysch unit of the Voirons-Wägital complex (Fig. 1). It is exposed at about 20 km from Geneva where it forms a series of smooth, wooded hills, the highest elevation of which reaching 1480 m (Signal des Voirons, Fig. 1). The Voirons Flysch is now subdivided into four formations (Ragusa, 2015):

1. The Voirons Sandstone Fm. is a sandstone-rich succession with a variable amount of intercalated marls. The basal part is dominated by marls with subordinate, cm- thick sandstone beds (Bons Sandstone Mb., Fig. 2A). Beds show recurring Bouma Tb—Te sequences (Fig. 2B). The remainder of the formation is dominated cm- to m-thick sandstone beds and marly intervals do not exceed a few cm in thickness. The base of the sandstone beds is commonly sharp, non-erosive, and sometimes bioturbated (Lombard, 1940). Some beds show rip-up clasts or mud-molds horizons (Fig. 2C). Isolated conglomerate layers occur along the Voirons crest (Fig. 2D). They are matrix-supported except for one clast-supported conglomerate. Initially considered as deltaic sediments (Lombard, 1940), the Voirons Sandstone Fm. is nowadays interpreted as channel and lobe deposits in a deep-sea fan (Ospina-Ostios et al., 2013; Ragusa, 2015). The boundary with the overlying Vouan Conglomerate Fm. is transitional (interfingering).
2. The Vouan Conglomerate Fm. mostly includes pebbly sandstones and poorly sorted, matrix-supported, conglomerates with a sandy matrix (Fig. 2E). Pebbles, cobbles and blocks are randomly distributed within the sandy matrix or constitute well defined horizons. The Vouan Conglomerate Fm. is mostly devoid of marly intervals. Marls usually occur as dm-sized soft pebbles. The dm- to m-thick conglomeratic beds have a limited lateral extent (Fig. 2F), and locally present a typical channel morphology. The Vouan Conglomerate Fm. thus is interpreted as channel deposits (Frébourg, 2006; Ospina-Ostios et al., 2013; Ragusa, 2015). The boundary between the Vouan Conglomerate Fm. and the overlying Boëge Marl Fm. is sharp.
3. The Boëge Marl Fm. is a marl-rich succession comprising rare, cm-thick sandstone beds (Fig. 2G). The latter commonly show partial (Tb—Te) Bouma sequences (Fig. 2H). The base of the formation locally includes dm-thick, matrix-supported conglomeratic layers, probably resulting from the collapse of the Vouan Conglomerate Fm. channels from upstream parts (Ragusa, 2015). The Boëge Marl Fm. is interpreted as distal lobe deposits (Ospina-Ostios et al., 2013; Ragusa, 2015). The sand-marl ratio progressively increases upward to the overlying Bruant Sandstone Fm.
4. The Bruant Sandstone Fm. (Ragusa, 2015) is lithologically similar to the Voirons Sandstone Fm. This unit only occurs in the Grande Combe – Tête de Char area. It was previously considered as a mélange (Kerrien et al., 1998) because of the important tectonic deformation near the boundary with the overlying Préalpes Médianes nappe

(Fig. 1). As the Voirons Sandstone Fm., the Bruant Sandstone Fm. is interpreted as channel to lobe deposits (Ragusa, 2015).

Initially dated from the Paleocene to Middle Eocene by nannofossil biostratigraphy (Jan du Chêne et al., 1975; Van Stuijvenberg, 1980), the Voirons Flysch is now attributed to the Early to Late? Eocene (Ujetz, 1996; Frébourg, 2006; Ospina-Ostios et al., 2013; Ospina-Ostios, 2017; Ragusa et al., 2018) on the basis of planktonic-foraminiferal associations. Provenance analysis (Ragusa et al., 2017) revealed two detrital sources of distinct composition in these deposits (Fig. 3). The “Quartzose petrofacies”, the main source, is a quartz-rich sediment with variable amounts of magmatic and sedimentary lithoclasts. The subordinate “Feldspathic petrofacies” essentially fed the Vouan Conglomerate Fm., but is also found as individual beds irregularly scattered in the other units of the Voirons Flysch. It comprises a feldspar-dominated assemblage characterised by inputs of metamorphic lithoclasts. These two petrofacies are respectively associated with a Clastic Wedge to Continental Block provenance (Quartzose petrofacies) and an Axial Belt provenance (Feldspathic petrofacies) following the model of Garzanti and Andò (2007). The Sesia-Dent Blanche nappes, the Briançonnais basement and the cover nappes already incorporated in the sedimentary accretionary prism are supposed to be the main detrital sources for both petrofacies. Petrofacies variations within the Voirons Flysch are related to either tectonic modification of the backstop or to climatic changes (Ragusa, 2015).

3. Methods

Geographic location of the outcrops, stratigraphic logs and datasets are available on the GitHub page of the first author (<https://github.com/jragusa/>) and in the electronic supplementary materials (framework composition and raw grain-size dataset). Dataset also includes few samples from the western part of the Gurnigel Flysch (Fayaux quarry).

3.1. Counting

The data previously obtained on the petrographic composition of the Voirons Flysch (Ragusa, 2015; Ragusa et al., 2017) are here reorganised in the following way. Quartz and feldspar grains are merged to avoid the influence of the provenance affiliation (Ragusa et al., 2017). Single grains (QFm) are separated from grains embedded in rock fragments and polycrystalline quartz (QFr) which can breakdown into smaller single grains. Extrabasinal lithics (L), originating from sedimentary, magmatic and metamorphic rocks, are separated from mudstone to wackestone fragments (Lc) interpreted as intrabasinal rip-up clasts (Ragusa, 2015; Ragusa et al., 2017). Red-algae (RA) and undifferentiated foraminifers (Fc), that form the most abundant intrabasinal skeletal grains, are detached from the other bioclasts (&Bc: echinoderm plates, spicules, bryozoan fragments). Intrabasinal non-calcareous grains include glauconite (Gl) and phosphate grains (Ph: undetermined phosphate grains and phosphatised foraminifers). Minor grains include micas (M) and dense minerals (D). The framework composition comprises also intergranular porosity (Pore) and cements (C), counted as equivalent grain. No matrix is reported in sandstones or is considered as negligible. Furthermore, we do not report clay flocculations. About 300 extrabasinal framework grains were counted whereas the amount of intrabasinal and interstitial grains varies from 7 to 577 depending on the sedimentary fabric, and especially the development of calcite cement. Missing values in the dataset are replaced by rounded zero of 0.001 value (Aitchison, 1986; Martín-Fernández et al., 2003). Sandstone classification uses the ternary diagram of Folk (1980).

3.2. Intergranular components

Calcite cement was stained with alizarin red-S and potassium ferri-cyanide (Dickson, 1965, 1966) to distinguish iron-free calcite (pink),

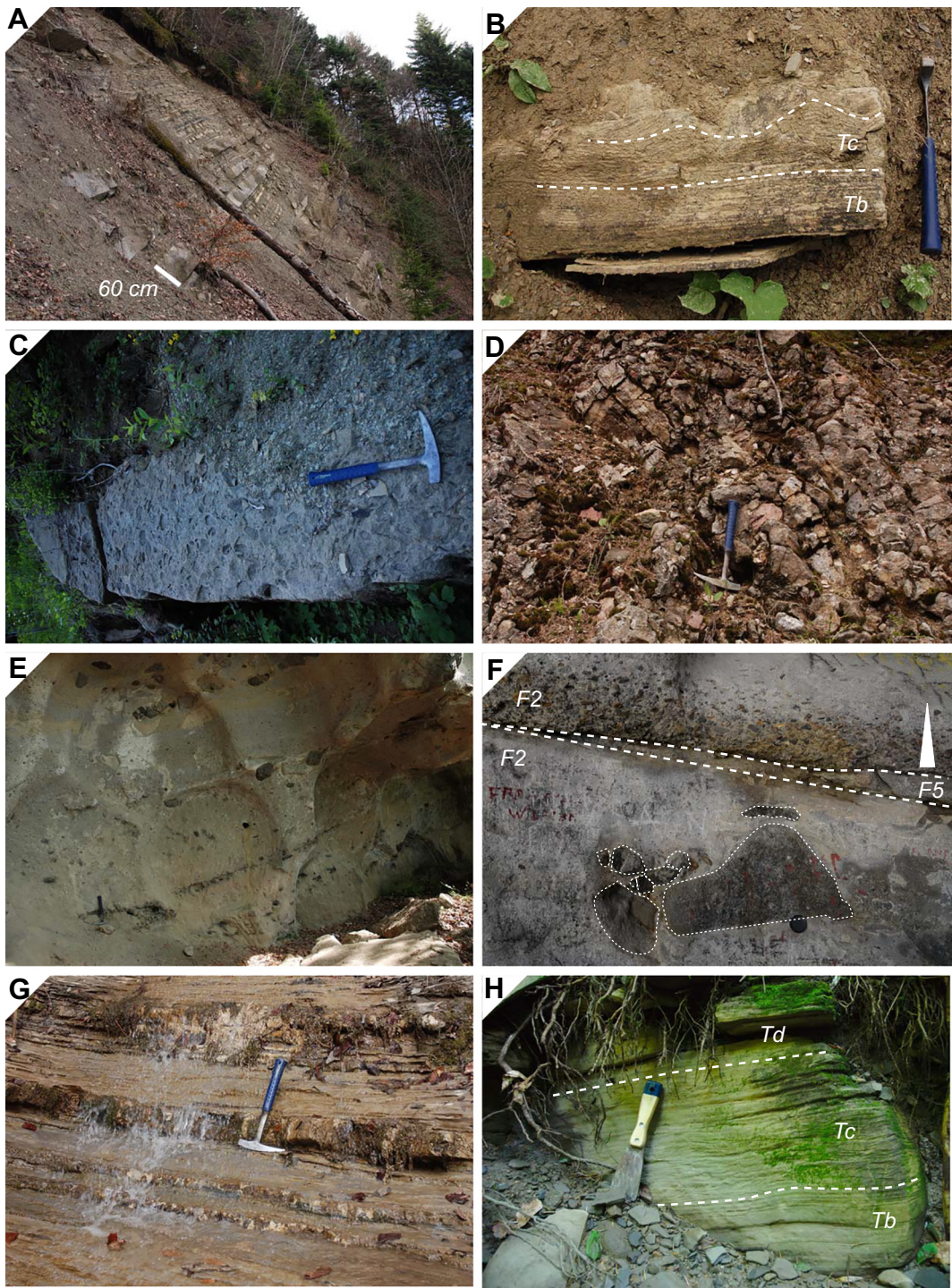


Fig. 2. Major features of the stratigraphic units of the Voirons Flysch: (A) marly interval of the Voirons Sandstone Fm. (N 46.2552 – E 6.39107), (B) Tb–Tc Bouma sequence in the marly interval, (C) mud mounds on the surface of sandy bed of the Voirons Sandstone Fm. (N 46.2281 – E 6.35851), (D) clast-supported conglomerate of the Voirons Sandstone Fm. (N 46.2281 – E 6.35851), (E) amalgamated beds of the Vouan Conglomerate Fm., notice the pebbly horizons (N 46.1754 – E 6.37718), (F) lateral variation (F5) within the Vouan Conglomerate Fm. associated to various pebble distribution (F2) (N 46.168 – E 6.38056), (G) marly interbed of the Boëge Marl Fm. in a stream (N 46.17 – E 6.38985) and (H) Tb–Td Bouma sequence in a sandy bed of the Boëge Marl Fm (N 46.1699 – E 6.38962).

iron-free dolomite (colourless), ferroan calcite (mauve to royal blue) and ferroan dolomite (turquoise). Cathodoluminescence microscopy (CL) was employed to analyse calcite cements and identify potential quartz cements and recrystallised calcareous grains. The CL analysis was performed using an ERI-MRTech-optical cathodoluminescence microscope with a cold cathode that was mounted on an Olympus BX41 petrological microscope. The beam conditions were 18 kV at 120–200 mA with an unfocused beam of approximately 1 cm. The

observation chamber has a residual pressure of ca 80 mTorr. The samples were non-coated.

The relative proportion of calcite cement and intergranular porosity are evaluated to assess their contribution to the interstitial voids. The latter is defined by the intergranular volume (IGV, Paxton et al., 2002) and corresponds to the sum of intergranular pore space, intergranular cement and depositional matrix (e.g. considered here as negligible). Considering that the whole Voirons Flysch was buried at approximatively

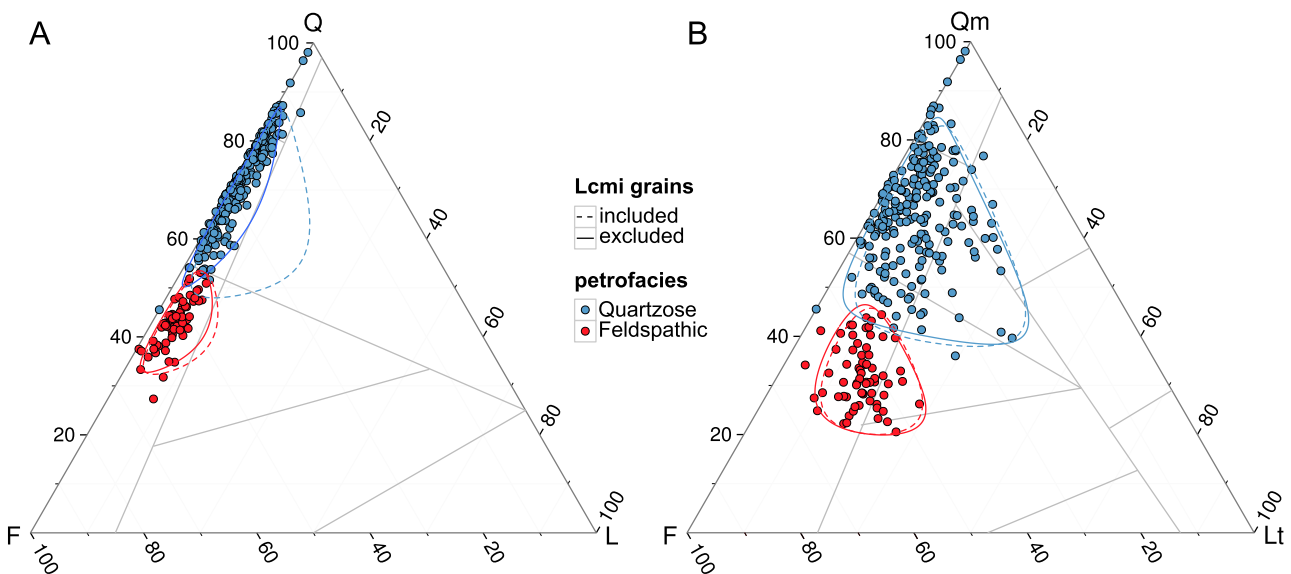


Fig. 3. Petrographic distribution in the QFL and QmFLt ternary diagrams of the Dickinson model (Dickinson and Suczek, 1979; Dickinson, 1985) from Ragusa et al. (2017, modified).

the same depth, the latter is precluded to explain different IGV values. We have also investigated the compactional porosity loss (COPL) and cementational porosity loss (CEPL) to discriminate the relative impact of the formers in the porosity loss of sandstone beds (Lundegard, 1992), assuming an initial porosity of 45%. Please note that samples were not impregnated with a colored medium for porosity determination which may underestimate the porosity volume. However, the contrast with stained feldspars and calcite minimises misidentification of pores.

3.3. Grain-size analysis

Grain-size measurement was made using a line-counting technique on thin sections (Blatt et al., 1980). Two hundred grains were counted per thin section to reduce the influence of sorting (Johnson, 1994). Several studies (Griffiths, 1967 and references therein) limited grain-size measurement to quartz grains. Indeed, several grains present specific hydrodynamic behaviour which can affect interpretations. For example, the tabular habitus of micas favours long-distance transport and a lower settling velocity than equivalent quartz grains (Doyle et al., 1983; Komar et al., 1984; Garzanti et al., 2008). Likewise, sand-size foraminifers are transport-equivalent to silt-size quartz grains due to their hollow structure (Oehmig, 1993; Jorry et al., 2006). Finally, ductile mudstone to wackestone lithoclasts were also removed because they can easily break-up during transport which influences their final grain size. The inclusion of feldspars and crystalline-rock fragments together with quartz grains is time saving, and overtakes the problem of limited counted grains in quartz-poor sandstones (Johnson, 1994). Results were converted to φ and reported according to the standard grain-size chart of Wentworth (1922). The upper and lower limits of counting are respectively defined at -2φ (gravel) and 5φ (coarse siltstone) by convention (Spencer, 1963; Dott, 1964; Johnson, 1994).

In contrast to loose sediments, grain-size measurement on thin section is made on 2D objects and has to be converted to 3D objects to estimate the true grain size. Several studies attempted to provide a reliable statistical conversion method by comparing sieving (real measurement) and thin section (estimation) (Friedman, 1958, 1962). Assuming ellipse-shaped grains, Johnson's method (Johnson, 1994; Friedman, 1996; Johnson, 1996) calculates the real diameter (D_φ) from the major (a'_φ) and minor axes (b'_φ), (Eq. (1)). Grain-size statistics are performed with the logarithmic method of moments (Blott and Pye,

2001) with 0.25φ class intervals and the relative percentages are based on the cumulative grain-size diameter of each interval.

$$D_\varphi = d'_\varphi - 0.4 \times (a'_\varphi - d'_\varphi) \text{ with } d'_\varphi = (a'_\varphi + b'_\varphi)/2 \quad (1)$$

3.4. Gravity-flow deposits

The sedimentary features of the studied gravity-flow deposits are described following the turbidite facies scheme of Mutti (1992, F2–F9). Identification and description of gravity flow mechanisms are based upon the nomenclature of Mulder and Alexander (2001).

3.5. Data processing

The combination of sedimentary features, grain-size and framework composition allows to group samples into several lithofacies (L1 to L6) (Table 1). Distribution is mainly based on the cluster analysis (Ward method and Euclidean distance) of the log-transformed framework composition (Aitchison, 1986). Their description is completed with the grain-size and the Mutti facies distribution (F2–F9). Computations and statistical analysis were performed using the R software (R Core Team, 2018). Principal component analysis is treated with factoextra packages (Alboukadel and Fabian, 2017). Samples distribution in ternary diagram is associated with fields indicating 90% confidence regions for the distribution, calculated via Mahalanobis distance and log-ratio transformation (Hamilton, 2017). Sample distributions are emphasised by linear model of regression, excepted LOESS regression (local regression) for Fig. 13A.

4. Results

4.1. Grain-size analysis

The mean grain-size of the sampled siliciclastic rocks from the Voiron Flysch (Fig. 4) is constrained between coarse sandstone ($\bar{x} = 0.29\varphi$, including the matrix of conglomerates) to coarse siltstone ($\bar{x} = 4.75\varphi$). Most samples present a unimodal and mesokurtic distribution except for some fine- to coarse-grained sandstones ($\bar{x} < 3\varphi$) with a platikurtic distribution (Fig. 4A). This latter group shows a bimodal distribution, comprising a major mode in the medium sandstone and a

Table 1
Major features of lithofacies.

Lithofacies	Name	Framework	Major composition	Interstitial grains	Grain-size	Depositional settings
L1	Poorly cemented medium (lithic-)arkose	grain-supported	QFm + QFr + L	Cement + porosity	Bimodal, poorly to moderately sorted	Channel (hyperconcentrated flow)
L2	Well cemented medium (lithic-)arkose	cement-supported	QFm + QFr + C	Continuous cement	Unimodal, moderately sorted	Channel (hyperconcentrated flow)
L3	Cemented medium (lithic-)arkose	grain to cement supported	QFm + QFr + L	Discontinuous cement	Unimodal, moderately sorted	Channel (hyperconcentrated flow)
L4	Highly cemented very fine arkose to calcarenite	cement-supported	QFm + C + Lc	Continuous cement	Unimodal, moderately sorted	Lobe (concentrated flow)
L5	Cross stratified planktonic-rich fine biosparite and very fine glauconitic arkose	cement-supported	C + QF + Fc	Continuous cement	Unimodal, moderately well sorted	Lobe (concentrated flow)
L6	Glauconitic quartzarenite coarse siltstone	grain-supported	QF + GI + Pore	Continuous cement	Unimodal, moderately well sorted	Reworked distal turbidite (turbiditic flow or bottom current)

secondary one in the very coarse sandstone to gravel range, separated by a grain-size break at ca. 0 ϕ (Fig. 5).

Sorting is negatively correlated with grain size (Fig. 4B): finer sediment being better sorted than coarser one. This confirms results from

modelling experiments (Lüthi, 1981; Komar, 1985) and from previous studies on gravity-flow deposits (Hubert, 1967; Piper, 1978; Holmes et al., 1987). Samples grade from poorly sorted to moderately well-sorted. Only siltstones reach the well-sorted grade. Moreover, sorting

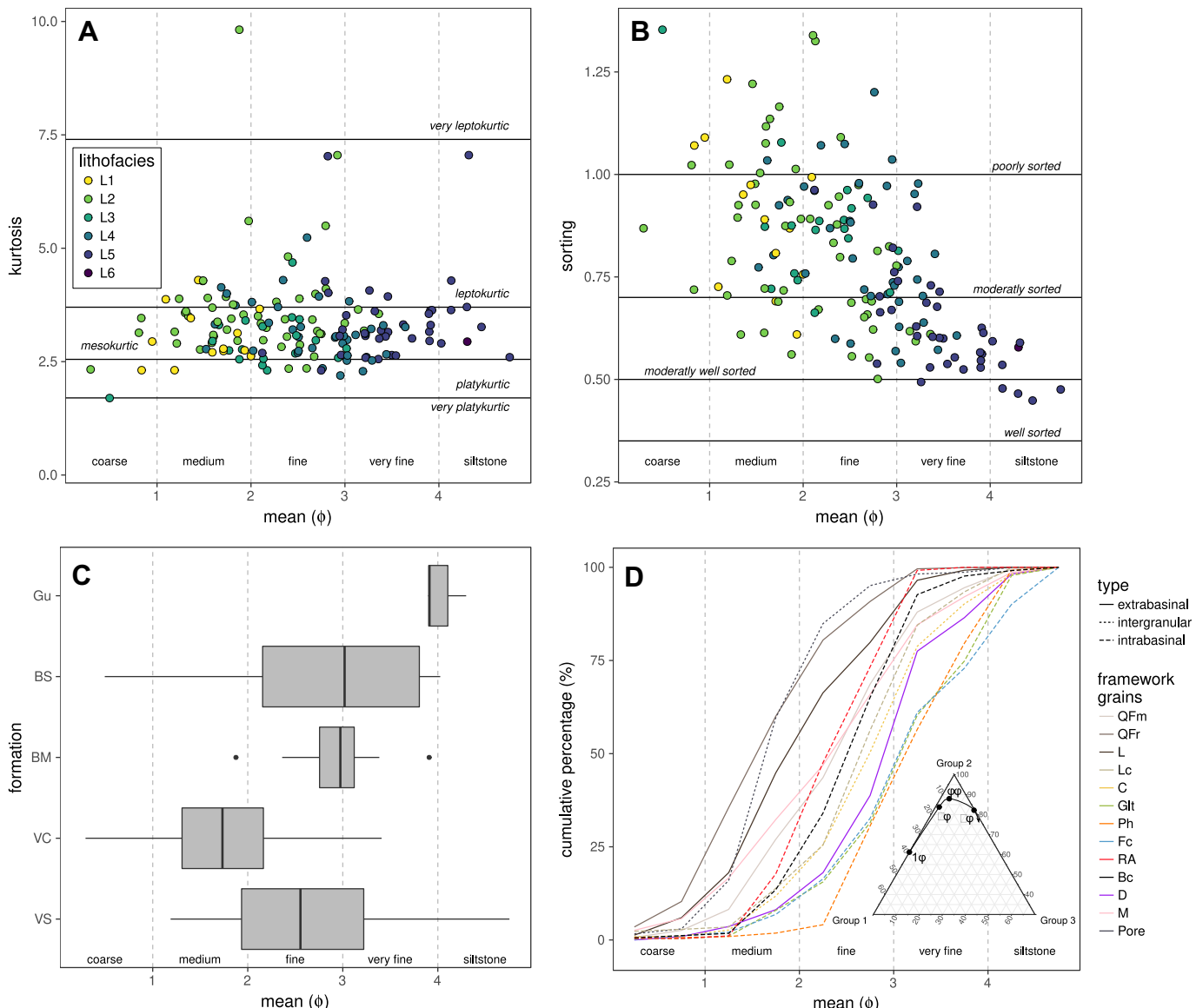


Fig. 4. Grain-size distribution of lithofacies: (A) mean vs. kurtosis, (B) mean vs. sorting, (C) mean grain-size distribution of each stratigraphic formation of the Voirons Flysch and (D) cumulative distribution of major grains identified.

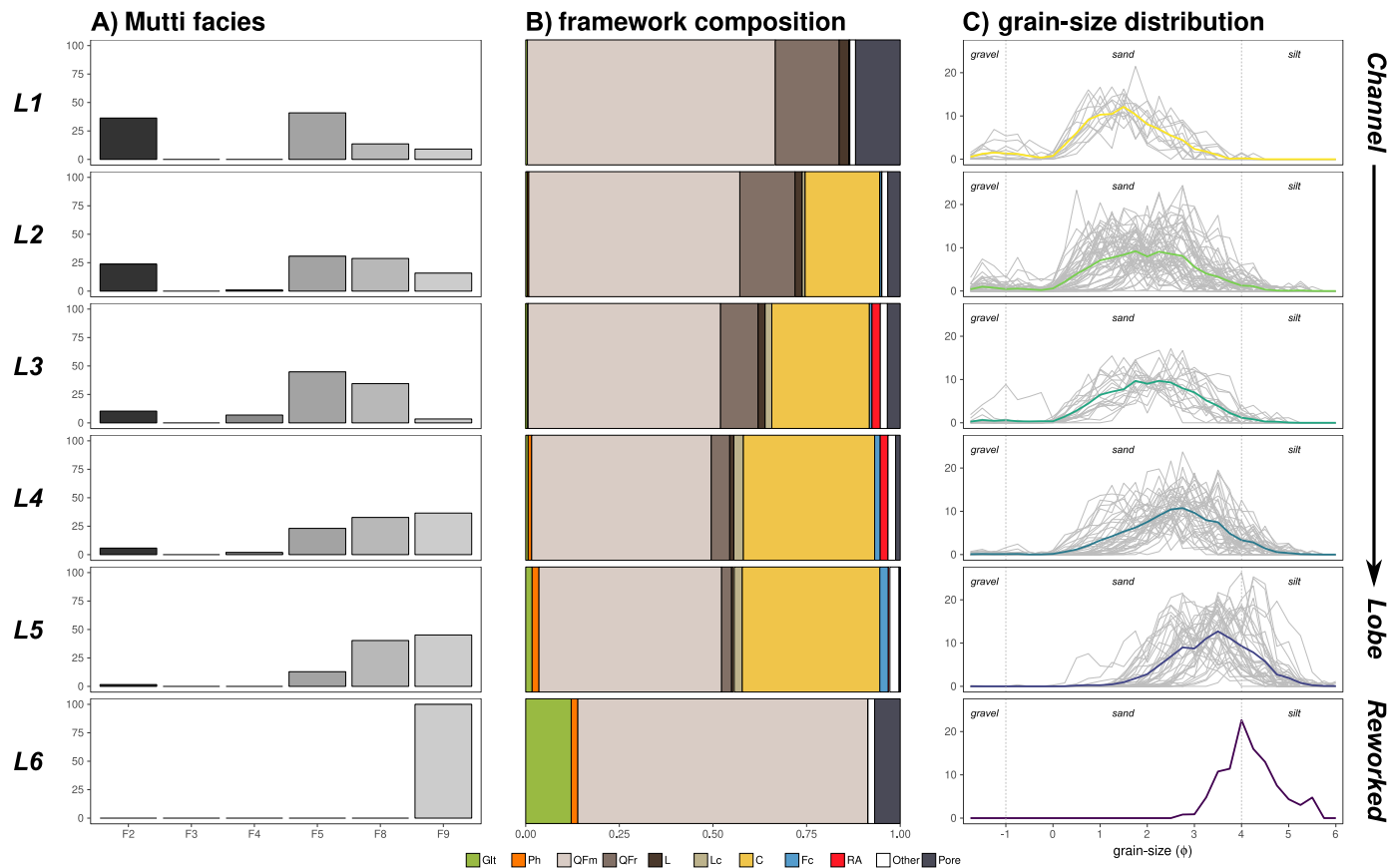


Fig. 5. Comparison of the lithofacies changes from the Mutti facies (A), framework composition (B) and grain-size distribution (C). Note the gradual evolution from channel to lobe depositional settings and the distinct features of the reworked deposits.

variation is highest in coarse sediments and significantly decreases in finer sediments. However, clay flocculation in the very fine sand and clay fractions may increase the sorting (Hubert, 1967; Stow and Bowen, 1980).

The Vouan Conglomerate Fm. includes the coarsest deposits with almost all samples located in the middle-sandstone range (Fig. 4C). They are poorly to moderately well-sorted (Fig. 4B). The Voiron Sandstone Fm. and the Bruant Sandstone Fm. display the largest grain-size variation. They mainly comprise moderately to well-sorted medium to very fine sandstones. The Boëge Marl Fm. is much more homogenous and comprises moderately to moderately well-sorted, fine to very fine sandstones. Finally, samples from the Fayaux quarry provide the finer distribution within very fine sandstone to coarse siltstone.

4.2. Framework composition

The Feldspathic petrofacies ranges from (lithic-)arkose to subarkose (Fig. 3) whereas the Quartzose petrofacies is constrained to subarkose. A few samples of the latter plot in the quartzarenite and litharenite fields. Reported to the sum of extrabasinal grains, quartz and feldspars show an antagonist behaviour (Fig. 6) which is emphasised by the relatively low amount of lithics (Fig. 3). The proportion of quartz grains increases while feldspars are progressively depleted. Their respective concentrations overlap themselves in coarse to medium sandstones and are well discriminated from fine sandstones, reaching a 75/25 ratio in coarse siltstone.

Detrital grains are poorly affected by diagenesis. Feldspars are weathered in various grades but there is no evidence of complete replacement. However, a partial depletion of feldspars by dissolution could have occurred without leaving evidence in deep buried open

systems, as pointed out by Milliken (1988). Some grains fractured by calcite are reported in a few thin sections and suppose an early stage of replacement. An albitisation process is also suspected (Ragusa et al., 2017) and would suppose a higher weathering grade (Milliken, 1988; Mu et al., 2016), related to the subduction of the Voiron Flysch in the accretionary prism, although an inherited origin cannot be excluded (González-Acebrón et al., 2010).

The intergranular volume (IGV) shows a positive correlation with grain-size (Fig. 7). The coarser deposits contain a low IGV (>20%), whereas grains are well spaced in finer layers with an IGV of 40–60%. Since sorting is positively correlated with the mean grain-size (Fig. 4B), the IGV also describes a positive correlation with the sorting as pointed-out by Paxton et al. (2002). It should be noted that several samples contain IGV values falling behind 26% corresponding to the physical lower limit for compaction of rhombohedral grain pack (Paxton et al., 2002). Except for scarce recrystallised bryozoan fragments (Fig. 8), calcareous grains are also well-preserved suggesting large import of calcite cement with an eventual supply from the albitised feldspars (Morad et al., 2000). Cement is homogeneously distributed and does not occur as tight bodies (McBride et al., 1995).

4.3. Lithofacies

The cumulative frequency of the grain content (Fig. 4D) shows a gradual deposition of the different grain classes into three main groups. Group 1 almost accumulates *L* and *QFr* grains in the coarse to fine sand (median = medium sandstone). Group 2 mainly comprise *RA*, *QFm* and *M* grains in the fine to very fine sandstone (median = fine sandstone). Finally the group 3 constituted by *Fc*, *Ph* and *D* (mostly zircon) grains is concentrated in the fine to very fine sandstone (median = very fine

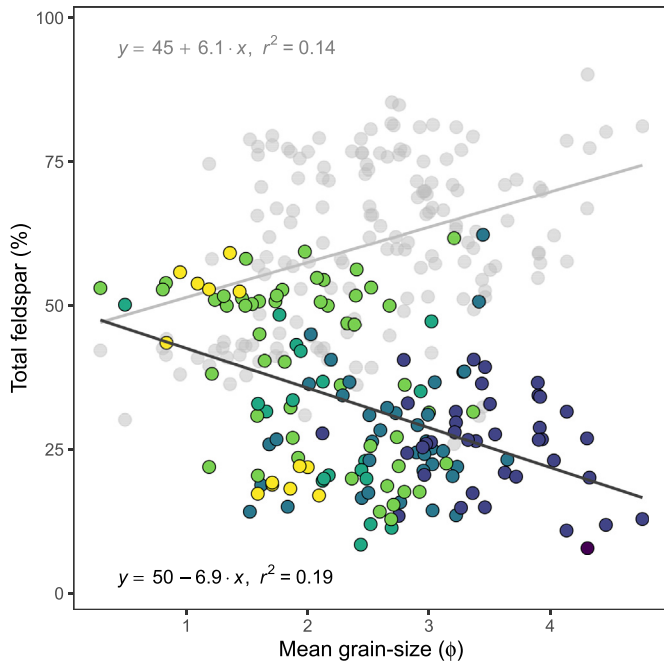


Fig. 6. Relation of the feldspar content with the mean grain-size. The feldspar content is computed from the total extrabasinal component. The quart content is depicted in grey shades for comparison. Note the antagonist behaviour of both components. Please refer to Fig. 4 for colour caption.

sandstone). Each depositional group is separated by a range of 1ϕ at the median to each other.

Based on the framework composition, the cluster analysis reveals five groups organised in two main branches (Fig. 9) and refined into six lithofacies (L1 to L6). QFm grains and cement (C) are the main contributors of the cluster distribution. The respective Mutti facies and grain-size distribution are attached to the facies (Fig. 5) and the main characteristics of each lithofacies are summarised in Table 1.

4.3.1. Poorly cemented medium-grained (lithic-)arkose (L1)

L1 outcrops consist of thick, sandy to conglomeratic successions assigned to F2 to F5 (Fig. 5). Erosive bases frequently occur. Shaly

intervals are generally absent, but scarce mud pebbles may be found. The sorting (Fig. 4B) is poor to moderate due to the bimodal grain-size distribution (Fig. 5). The main group is centred on the medium-sandstone size. The other one, of the gravel size, corresponds to the conglomeratic layers found in the Voiron Sandstone and the Vouan Conglomerate formations.

The framework grains mostly comprise quartz and feldspar (Fig. 10A). The main lithic fragments are crystalline grains. Lc grains are rare as well as other intrabasinal grains. The poor sorting results in significant porosity development which is sometimes filled by calcite cement (Fig. 10B). Pressure-dissolution features are abundant (Fig. 10A). Labile grains are bent (micas) or abraded (foraminifers) by surrounding particles (Fig. 10C). The extensive grain contact and scarce cement results in a very low IGV (1–26%), mostly represented by porosity (Fig. 7). These values, lower than 26%, corroborate the extensive grain interpenetration (Paxton et al., 2002). Contacts between grains are so tight that the distinction between single grains and polycrystalline grains is sometimes difficult. No quartz cementation was observed between detrital grains and is considered as insignificant.

4.3.2. Well-cemented medium-grained (lithic-)arkose (L2)

L2 exposures show stacks of thick sandstone beds with rare shaly intervals. The grain size is mostly concentrated in a single mode centred between the medium and fine sandstones. Residual secondary peaks are localised in the gravel-size (Fig. 5). Sorting remains moderate despite a likely unimodal grain-size distribution (Fig. 4B).

The framework composition is dominated by siliciclastic grains (Fig. 5): quartz, feldspars (QFm + QFr grains) and crystalline lithoclasts (L grains). The framework remains grain supported although ferroan calcite cement greatly increases and fills most of the porosity (Fig. 10D). Labile grains are carved. Skeletal-grain content is low. It includes large benthic foraminifers (nummulitids and discocyclinids), bryozoan and coarse red-algae fragments. Rare shark teeth occur also. Most bioclasts are fragmented and indented by adjacent grains. In samples with a notable content of skeletal grains, displacive cement greatly increases the IGV (2–59%, Fig. 7) and floating grains occur locally (Fig. 10D).

4.3.3. Cemented, medium-grained (lithic-)arkose (L3)

The sedimentary features seen on L3 exposures are similar to those of L1. Beds present also erosive bases, and lateral variations are similarly

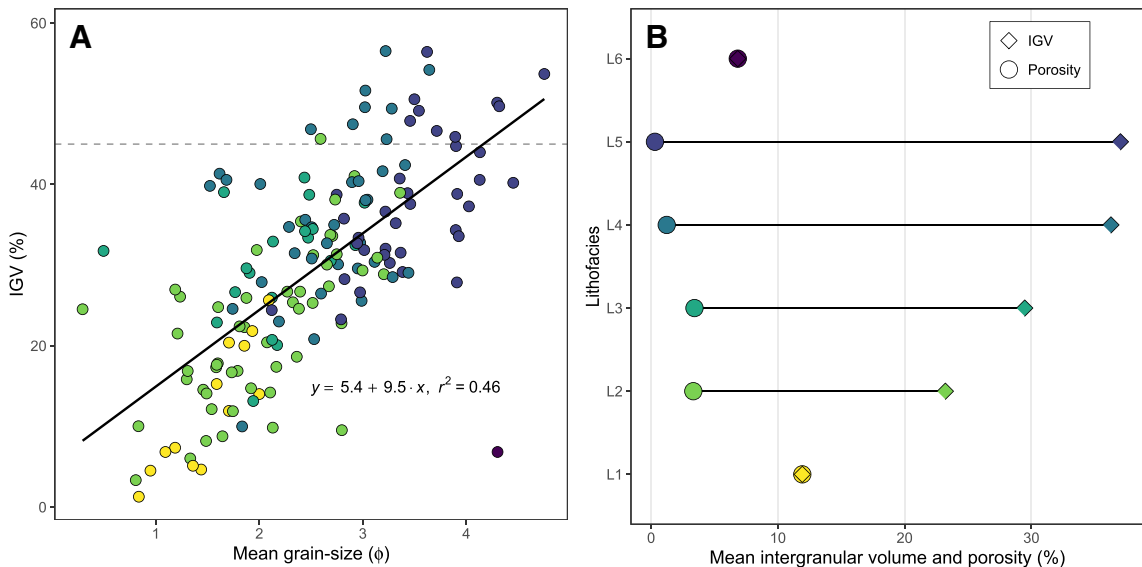


Fig. 7. Interstitial component. (A) Relation of intergranular volume (IGV) with mean grain-size. The dashed line correspond to the initial porosity of 45% used to compute the IGV. Values above this line indicate floating grains and potentially highest value of initial porosity. Note the isolated location of lithofacies L6. (B) Relation between the mean IGV and mean porosity of each lithofacies. More the points are separated more the IGV is filled by calcite cement. Please refer to Fig. 4 for colour caption.

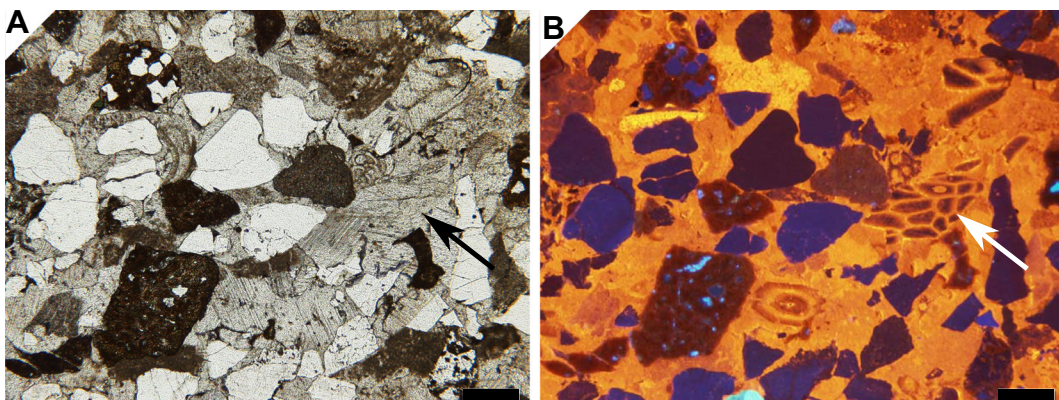


Fig. 8. (A) Natural light and (B) cathodoluminescence photos of JR235 showing recrystallised bryozoan. Stained feldspars are yellow to reddish. Notice the homogeneous calcite cementation and lack of zonation. In highly cemented facies, grains are isolated and bathe within calcite cementation. The arrow shows a recrystallised bryozoan. Scale bar represents 200 µm. (For interpretation of the references to colour in this figure legend, the reader is referred to the web version of this article.)

reported. F8 to F9 are the most frequently observed facies with subordinate F2 to F5. Beds can be amalgamated and are commonly dm- to cm-thick. The nearly unimodal distribution is located in the median to fine sandstone. The gravel-size component is still low. Sediments are moderately sorted (Fig. 4B).

The siliciclastic content remains the dominant fraction but decreases at the expense of the calcite cement (Fig. 5). This increase mainly consists of porosity filling and does not affect the framework properties previously described (Fig. 10E). However, the cement content is lower than in L2. A better sorting related to the decreasing mean grain size favours a better preservation of the initial porosity mostly filled by cement. The calcite cement is patchy (Fig. 10E). Hence, L3 maintains a grain-supported framework. Grain contacts are common, and labile grains are deformed or corroded. Intrabasinal precipitates (glauconite and phosphate) are rare. The proportion of calcareous lithoclasts is low and those of red-algae fragments increases. The IGV values is relatively high (10–43%) whereas the porosity remains low (Fig. 7), indicating that most of the IGV is filled by calcite cement.

4.3.4. Well-cemented, fine-grained arkose to calcarenite (L4)

L4 exposures typically show F8–F9. They consist of cm-thick sandstone beds alternating with sandy marls, representing the typical flysch lithology. Sediments are fine- to very fine-grained, moderately to well sorted and show a unimodal distribution (Figs. 4B and 5C).

The framework composition is dominated by the siliciclastic component followed by calcite cement (Fig. 5). Calcite cement is so abundant that grains become isolated and the framework is cement-supported (Fig. 10F and G). Some grains are fractured and filled by ferroan calcite.

This abundant cement preserves bioclasts and other labile grains (Fig. 10H). Calcareous grains are rare and mostly comprise lithic gains (Lc). Skeletal grains are also rare. Foraminifers are the most abundant bioclasts. They present a large diversity including both benthic and planktonic species (Fig. 10H). Several samples show an IGV greater to 45% (9–57%, Fig. 7) indicating than floating grains occur frequently, embedded in a large displacive calcite cement.

4.3.5. Cross stratified, very fine-grained glauconitic arkose (L5a) and planktonic-rich, fine-grained biosparite (L5b)

Beds of L5 and L4 lithofacies commonly occur on the same exposures. They consist of cm-thick sandy beds of F5 to F9 and interspersed with marly intervals. L5 includes moderately well- to well-sorted, very fine-grained sandstone to siltstone (Fig. 4B). Calcite is the most abundant fraction followed by the siliciclastic fraction (Figs. 5 and 10D). Based on the total carbonate amount, L5 can be described as a calcarenite or a calcilutite. Sedimentary lithoclasts are the most abundant clasts and crystalline-rock fragments are scarce. Planktonic foraminifers are the third most important group. Benthic foraminifers are missing. Glauconite is frequent. Sedimentary features describe either a massive unit or mm-scale, cross-bedded laminae capped by soft-deformation convolute (Fig. 11A). These laminae consist of an alternation of yellow and brown layers (Fig. 11A and B) reflecting two different compositions, clearly highlighted by cement staining (Fig. 11B and C): (L5a) siliciclastic laminae consisting of a glauconite-rich quartzarenite to subarkose with micas, patchy to widespread ferroan-calcite cement, and (L5b) planktonic foraminifer-rich biosparite with few siliciclastic grains. Foraminifers are well-preserved and form stacks of tests interspersed by some micritic grains. Cement fills the moldic porosity. The overall yellow tone and composition is reminiscent of the Alberese facies described by Studer (1827). Several samples show an IGV greater to 45% (22–57%, Fig. 7) indicating than floating grains are frequently embedded in large displacive calcite cement.

4.3.6. Glauconitic fine-grained quartzarenite to siltstone (L6)

Only one bed of this assemblage has been found in the Voirons Flysch (Fig. 11D) but similar sandy beds have been documented in the remainder of the Voirons-Wägital complex (Van Stuijvenberg et al., 1976). They are localised at the base of the flysch units within marl-dominated intervals. The rare occurrence of these green sands limits outcrop description. The sedimentary features suggest a F9.

The grain-size distribution indicates a moderate sorting between very-fine sandstone and siltstone (Fig. 5). The important glauconite content (12.15%, Fig. 5) is reflected by the green shade of the bed (Fig. 11E).

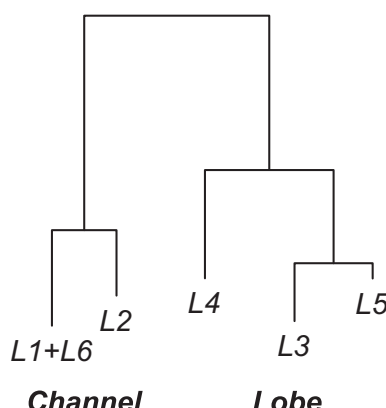


Fig. 9. Simplified cluster diagram showing the lithofacies distribution.

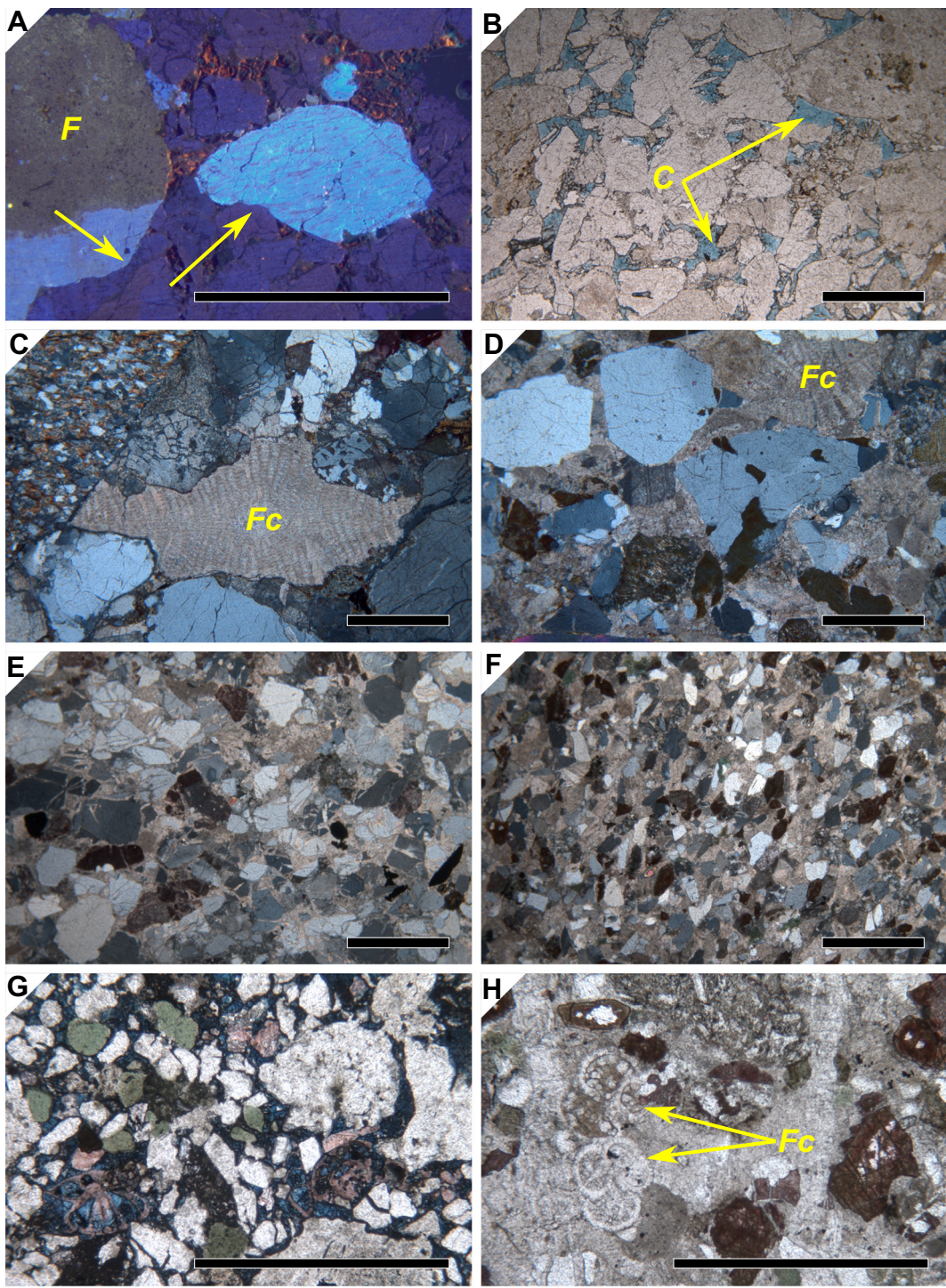


Fig. 10. Major petrographic features of lithofacies L1 to L4. (A) CL image of lithofacies L1 with large grain contacts and pressure-dissolution (arrows). (B) Intergranular porosity filled by ferroan calcite in L1. (C) Abraded large planktonic foraminifera (*Fc*) in L1. (D) Petrographic framework of L2. (E) Petrographic framework of L3. (F) Cement-supported petrographic framework of L4. (G) Continuous ferroan calcite cementation in L4 and (H) well preserved pelagic foraminifers (*Fc*) in L4. Scale bar represents 500 µm.

The different shapes and hues of glauconite suggest different origins (Fig. 11F). The framework composition only comprises quartz and glauconite in decreasing order (Fig. 5). Phosphate grains and micas represent minor components. The fabric is characterised by the numerous grain contacts which favours a significant porosity (Fig. 11E). Pressure-dissolution features are frequent. The lack of cement, the large content in glauconite and the very fine grain-size suggest contrasting depositional settings. Although located in the same cluster as L1, L6 is similar to the glauconitic quartzarenite laminae of L5a (Fig. 11B and C).

Lithofacies L6 shares also with L1 a very low IGV (6.83%, Fig. 7) mainly composed of porosity.

5. Discussion

5.1. Compositional variation

Although Mutti's classification and the grain-size distribution were not included in the cluster analysis, a close relationship appears

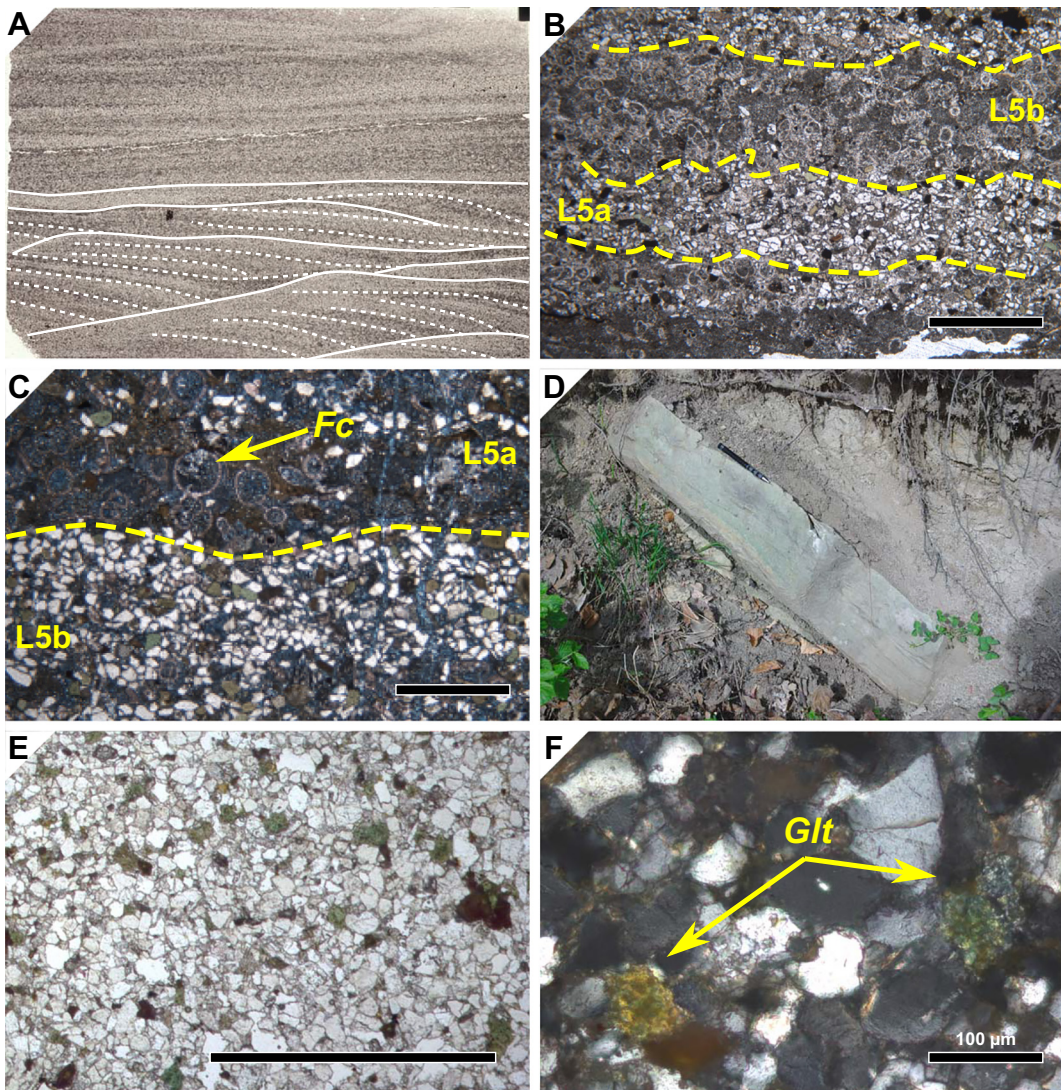


Fig. 11. Major petrographic features of lithofacies L5 and L6. (A) Macrophotography of cross-bedded framework topped by convolutes in L5 (width = 30 mm). Continuous and dashed lines correspond to set and foreset, respectively. (B) Microscopic view of the light glauconitic-rich layer (L5a) and dark bioclastic-rich layer (L5b) of L5. (D) Closer details of L5a and L5b layers of L5 with calcite stained. The calcite staining better emphasises the different compositions of layers. (D) Green bed of L6 and (E) petrographic framework of L6. (F) Yellowish and green glauconite (Glt) from L6. Scale bar represents 500 µm. (For interpretation of the references to colour in this figure legend, the reader is referred to the web version of this article.)

between these characteristics and the framework composition of each lithofacies (Fig. 5). A principal component analysis (Fig. 12) focusing on the framework composition and the mean grain size confirms this trend (Figs. 13 and 14). Basinward, sediment sorting evolves from poorly to well-sorted. Alongside, the framework composition grades between two end members, separated by two segregation stages (Figs. 4D and 14): (1) the extrabasinal polycrystalline grains (*QFr* and *L* grains) abundant in coarse to medium sandstones (L1–L3; group 1) are progressively replaced by monocrystalline grains (*QFm* grains) in fine sandstones (L4–L5; group 2); (2) the dominant extrabasinal monocrystalline grains (*QFm*) in fine sandstones (L4) decrease and are concurrently replaced by intrabasinal calcareous (*Bc*, *Fc*, *RA*, *Lc*) and authigenic grains (*Ph* and *Glt* grains; L5; group 3, Fig. 4). Hence, gravity-flow deposits grade basinward from a pure extrabasinal siliciclastic composition in proximal settings to a more intrabasinal calcareous composition in distal settings, thus confirming the studies of Stanley (1963), Fontana et al. (1989) and Zuffa (1991). In a similar way, the coarsest lithologies from the proximal area are characterised by the preservation of porosity (L1) whereas porosity loss by cementation increases notably in fine sandstones (Fig. 15), simultaneously with the relative increase of bioclasts (*Fc*, *RA* and *Bc* grains; L4–L5).

Mica grains show however a different behaviour. Their proportion is independent to the mean grain size (Fig. 12), and they are reported in both coarse- and fine-grained sediments. Coarse mica flakes are more easily trapped upstream in the coarse layers whereas fine micas migrate efficiently upward in the flow and concentrates basinward. Their widespread occurrence may reflect also disturbances caused by the hydraulic regime of gravity flows (Komar et al., 1984) or neoformation during diagenesis (dos Anjos et al., 2000). This result differs from those of previous studies (Stanley, 1963) stating that micas are preferentially concentrated within fine-grained sediments because they present a lower settling velocity than equivalent quartz grain (Doyle et al., 1983; Komar et al., 1984; Burroughs, 1985; Doyle et al., 1985).

Heavy minerals are positively correlated with the fine fraction as shown by the large content in zircon and rutile (Ragusa et al., 2017). Due to their greater density, these grains are likely fine grained. This does not agree with most previous research, according to which dense minerals are always found with coarser equivalent grains (Garzanti et al., 2008) and their content decreases downstream (Norman, 1969). Such a fine grain-size is probably linked to (1) limited availability of coarse grains in source rocks (Stanley, 1963; Morton and Hallsworth, 1999; Garzanti et al., 2008), (2) hydrodynamic fractionation (Morton and Hallsworth,

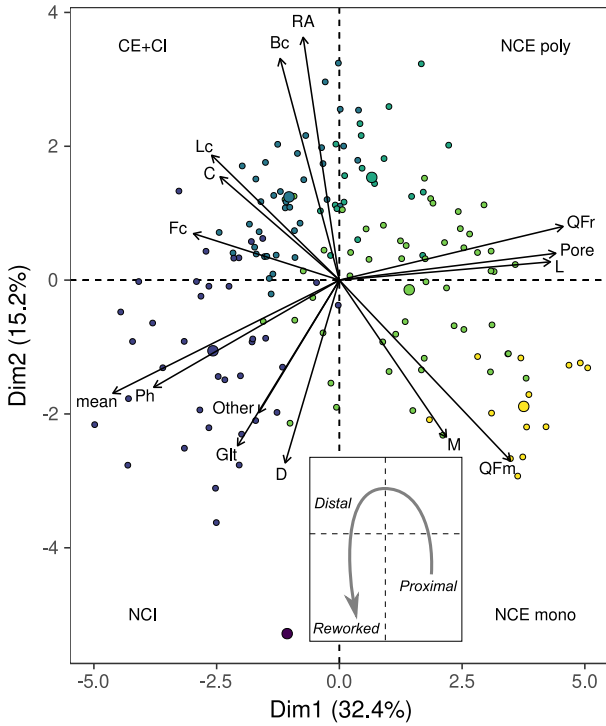


Fig. 12. PCA diagram of framework composition and mean grain-size. Please refer to Fig. 4 for colour caption.

1994, 1999), and/or (3) the predominance of reworked fine grains yielding an older age (Lawrence et al., 2011; Yang et al., 2012). Norman (1969) also suggested that proximal parts comprise more mineralogical variations, but the very low heavy-mineral content (<1%) precludes an accurate estimation (Ragusa et al., 2017). In addition, the transport mechanisms may favour localised accumulation (e.g. placer) in relation to the sedimentary features (Zimmerle, 1973; Cheel, 1984; Garzanti et al., 2015).

5.2. Depositional settings

On the basis of the previously described parameters (Fig. 5 and Table 1), a depositional model (Fig. 15) of detrital grains in relation

with the flow dynamic and the inherited diagenesis is proposed in which we distinguish channel (L1 to L3), lobe depositional settings (L4 and L5) and a reworked facies (L6). Although located with L4 and L5 (Fig. 9), L3 may correspond to a transitional facies between channel and lobe. Overall, the abundant calcareous grains and cementation, especially in the distal petrofacies corroborates a deposition above the CCD (Hesse and Butt, 1976).

5.2.1. Channel (L1–L3)

In the upstream part of the flow, large clasts are easily transported (Postma et al., 1988; Fig. 15). They characterize the conglomerates and pebbly sandstones (Fig. 2E and F) of the Vouan Conglomerate Fm. and those along the crest of the Voiron massif. The lower portions of flows mostly contained siliciclastic components, including a large proportion of polycrystalline grains (QFr, and L grains), whereas lighter grains migrate upward in the upper flow layers. However, this upward transport is not fully efficient, as shown by the large mode of grain-size curves (Fig. 5). Rare light grains, such as skeletal grains and micas, are trapped within the basal layer. They generally migrate in the upper layers due to their porosity and easier traction ability. These deposits are preferentially related to hyperconcentrated density-flows (Mulder and Alexander, 2001), characterised by grain-to-grain interactions and corresponding to F2–F5, whereas F8–F9, observed in lithofacies L1 to L3, may correspond to overbank deposits.

The very low IGV (Fig. 7A) associated with the low proportion of cement and the occurrence of stacks of m-thick beds suggest that mechanical compaction was the main diagenetic control. This is confirmed with the porosity loss parameters of Lundegard (1992). Most of samples describe a predominant compactional porosity loss with no to minor cementational porosity loss (Figs. 7B and 16) as depicted by Lundegard (1992). This compaction is easily transmitted to the lower beds due to the lack of notable shaly layers to absorb compaction and fluid overpressure (Bloch and Lander, 2002). Within the framework composition, sutured contacts are frequent between quartz and feldspar grains (Fig. 10A), but stylolites are missing. Overall, further chemical compaction (pressure-dissolution) could lead to the development of a quartz cement or during an early stage of burial (Paxton et al., 2002). Micas, fine-grained sedimentary rocks (phyllite and siltstone) and schistose metamorphic lithoclasts are bent by rigid grains. Likewise, the scarce bioclasts (e.g. large benthic foraminifers) are extensively indented by the adjacent grains (Fig. 10C). The low percentage of cement is frequent in channel settings (Moares and Surdam,

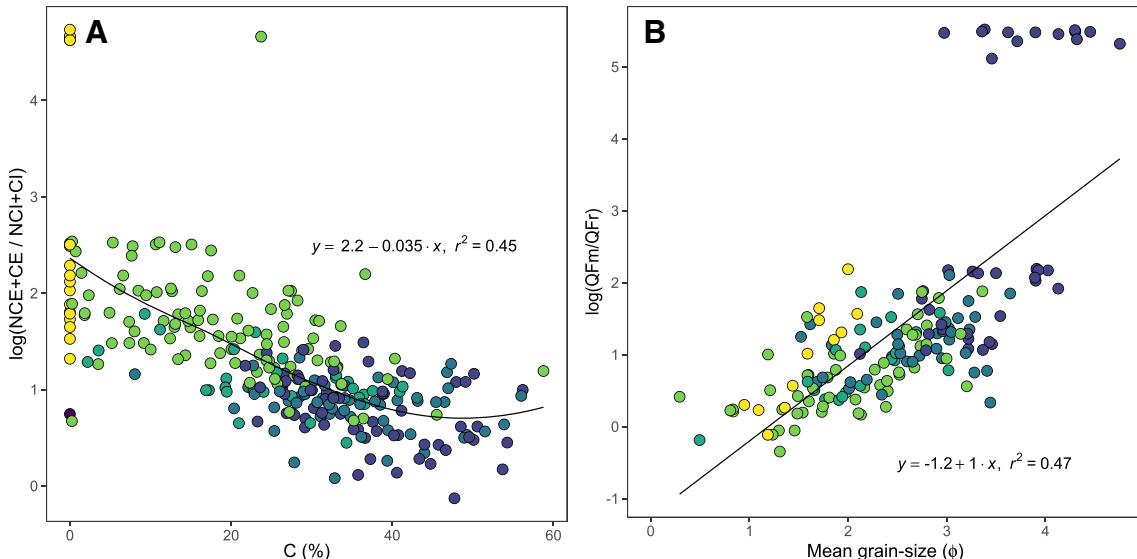


Fig. 13. Evolution of the framework grains content with lithofacies. (A) framework composition (intrabasinal vs extrabasinal) vs. cement, and (B) ratio of extrabasinal single grains over embedded grains in rock fragments vs. mean grain-size. Please refer to Fig. 4 for colour caption.

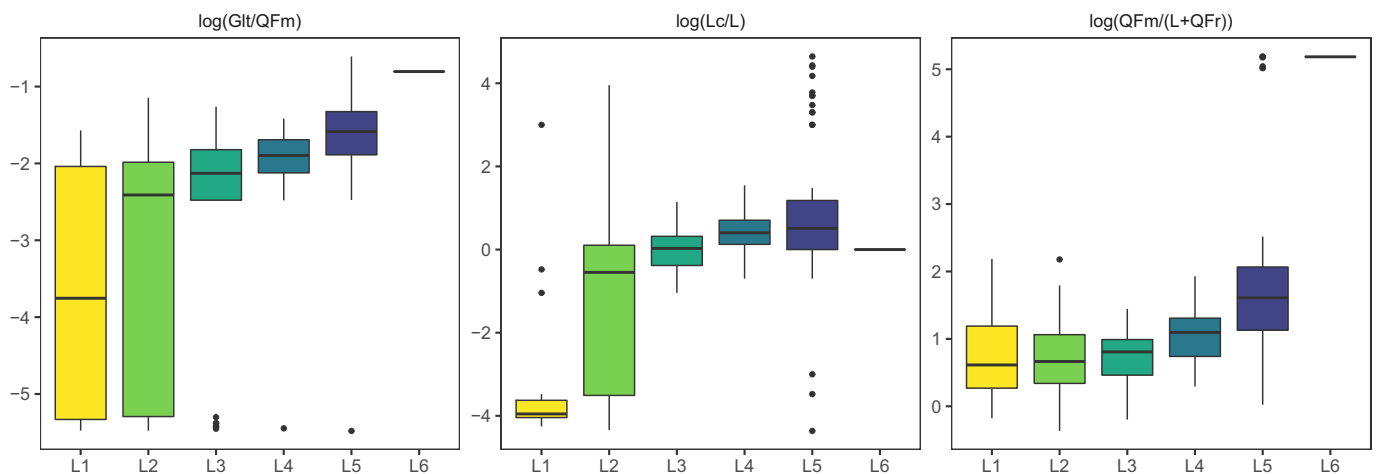


Fig. 14. Main ratio of the framework grains showing the basinward evolution of the detrital composition. Please note the overall increase from channel to distal deposits (L1-L5) and the break with L6.

1993). The poorly sorted, porous, coarse-grained sandy deposits of L1 represent a prime target for hydrocarbon exploration (Stow and Mayall, 2000; Bloch and Lander, 2002). As the main diagenetic control, compaction preferentially affects labile grains (Milliken, 2001; Bloch and Lander, 2002; Paxton et al., 2002). They may be transformed (Dickinson, 1970) disturbing the detrital signal. Therefore, fluid circulation, enhanced by the primary porosity, might have contributed to dia-genetic alterations (Morad et al., 2000). Hence, dissolution of ferromagnesian minerals likely produced authigenic micas (dos Anjos et al., 2000).

Despite the compaction, the residual porosity is still important (Fig. 7) due to the quartzose composition and the lack of quartz cement (Reed et al., 2005; Mansurbeg et al., 2009). Basinward, poikilotopic calcite cement fills the porosity (L2 and L3, Fig. 7). Although there is no evidence of nucleation from carbonate grains and rare carbonate grain dissolution (Fig. 8), we observe a positive correlation of bioclasts with calcite cement (Figs. 12 and 13A). It is also should be noticed that the ratio extrabasinal vs. intrabasinal component increases in very cemented sandstones (Fig. 13A) which could suggest local dissolution of carbonate grains. Consequently, most of calcite cements seem to be imported (open system). Chemical intrabasinal grains (glauconite and phosphate) are rare since they are transported far away in the distal parts (Amorosi, 1997). The short timespan between successive gravity flows in the upstream part may also explain their low amount.

5.2.2. Lobe (L4–L5)

These deposits present many sedimentary structures typical of sub-critical flows (lower plane beds, ripples, convolute) associated with F8–F9. In fine-grained deposits, the repetitive pattern of mm-scale, cross-stratified laminae (Fig. 11A) is frequently observed. Overall, they likely resulted from density to turbidity currents (Mulder and Alexander, 2001), whereas the cross-stratified laminae may correspond to pulsations in the turbidity flow or to repetitive, short-duration depositional events, such as surge-like flows (Mulder and Alexander, 2001). Similar deposits observed in the Ultrahelvetic realm (Hsü, 1964) and in the Niesen Flysch (Bouma, 1972, 1973; Stanley, 1993) (Fig. 1) were tentatively interpreted as fossil contourites, but this interpretation remains controversial (Stow et al., 1998, 2002).

Crystalline-rock fragments (QFr and L grains) decrease rapidly with the upstream deposition of the coarse fraction in the channel (Fig. 5). Extrabasinal crystalline rock-fragment are progressively replaced by intrabasinal micritic clasts eroded from the sea floor (rip-up clasts) (Lc/L ratio, Fig. 14). Although, the relative distribution of quartz and feldspars is influenced by the provenance (Ragusa et al., 2017), their relative proportion depicts an opposite evolution with an increasing

content of quartz while feldspars are progressively depleted (Fig. 6). This evolution corroborates previous findings in river sediments (Garzanti, 1986; Milliken, 1988) and the proportion of feldspars remains significant in the coarse silt fraction (ca. 25% of the extrabasinal component). However, we do not find any behaviour suggesting a better preservation in finest fractions as postulated in previous publications (Milliken, 1992). Further sorting operates within the foraminiferal assemblage (Figs. 12 and 15). Large benthic foraminifers are preferentially deposited upstream (Fig. 10C and D), whereas planktonic foraminifers appear in L4 and represent the only group of foraminifers in L5 (Fig. 11B and F). Such progressive loss of rock fragments in finer grain size is largely documented in various settings (Tolosana-Delgado and von Eynatten, 2009, references herein). Alternatively, the weak crystal boundaries of L grains may contribute by mechanical disaggregation to the monomineralic composition (QFm grains) (Grantham and Velbel, 1988; Johnsson, 1993).

The large upstream deposition of the siliciclastic component concentrates grain of greater transport ability such as skeletal grains and especially foraminifers (Figs. 5, 12 and 15) (Brunner and Normark, 1985; Oehmig, 1993; Jorry et al., 2006). They are trapped and corroded in the upstream part and especially in channel depositional settings (Weidmann, 1967; Kuenen, 1968).

In the finer sediments, the very low velocity marks a clear threshold between the dense fraction including monocrystalline siliciclastic grains and glauconite forming the light laminae (L5a), whereas the light bioclastic grains (foraminifers) of the turbulent cloud aggregate in the dark laminae (L5b) (Figs. 11B, F and 15). Equivalent facies were reported by Scholle (1971) in distal deposits of the Monte Antola Formation (Italy). Additionally, micas can also form a major component because of their low settling velocity (Komar et al., 1984). Moreover, plant debris, frequently reported in the Voirons-Wägital complex (Lombard, 1940; Van Stijvenberg et al., 1976; Caron et al., 1989), confirm distal deposits (Kuenen, 1968; Zavala and Arcuri, 2016).

Grain contacts and compaction strongly decrease in distal environments. Lobe deposits are characterised by a great increase of the IGV which is mostly filled by the widespread calcite cement (Fig. 7). The latter is the major responsible of porosity loss (Fig. 16). However, 11 and 13 samples of lithofacies L4 and L5, respectively, show a negative COPL. For these samples, an initial porosity >45% is necessary (liquefied sand?) or suggest that displacive cementation increased the IGV with respect to the initial porosity. Consequently, the impact of compaction vanishes or is probably absorbed by the increasing proportion of adjacent marly intervals. These marly intervals (Fig. 2A and G) emphasize the increased timespan between depositional stages and promote precipitation of glauconite.

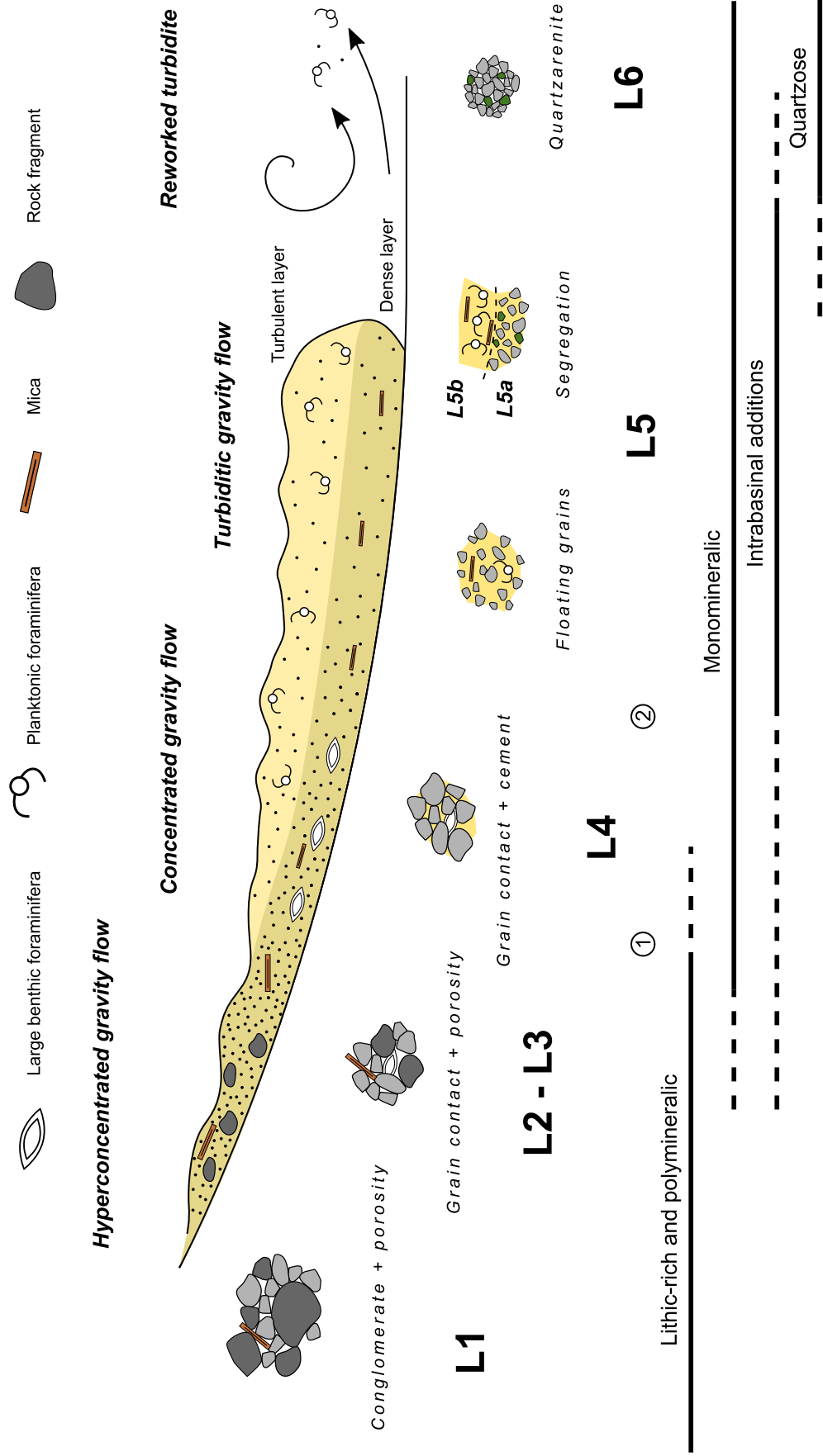


Fig. 15. Synthetic depositional model showing the compositional variation in gravity-flow deposits. 1 and 2 correspond to the major segregation stages. Note the gradual fining trend and increasing cementation basinward. Reworked turbidite is here interpreted as deriving from L5 lithofacies. Please refer to text for explanation.

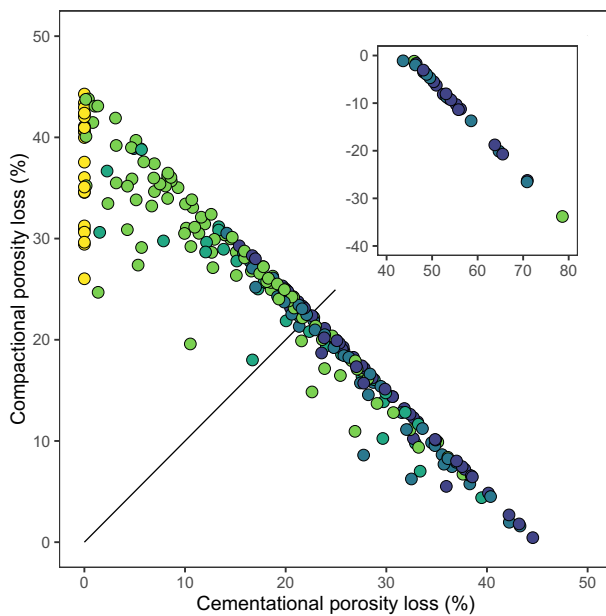


Fig. 16. Influence of compaction and cementation in the porosity loss following Lundegard (1992). The inset graph shows the samples with negative compactional porosity loss (COPL). Please refer to Fig. 4 for colour caption.

The large development of poikilotopic calcite cement occludes the original intergranular porosity (Figs. 8 and 10). Evidence of syntactic cementation is also reported in association with echinoderm plates suggesting localised nucleation. Except for scarce recrystallised bryozoan fragments (Fig. 8), calcareous grains are well preserved. The concomitant lack of extensive calcareous grain dissolution and restricted nucleation site suggest that calcite was mostly imported in an open-system. The important development of an early calcite cement limits post-diagenetic processes such as feldspar weathering (Morad et al., 1990). In our case study, the lack of zonation and the bright

orange-red luminescence of the calcite cement (Fig. 8) suggest an early pore-filling poikilotopic cementation (Kim et al., 2007). The low recrystallisation rate also indicates that calcareous grains do not contribute to the cementation by dissolution (Bjorkum and Walderhaug, 1990) (Fig. 8).

5.2.3. Reworked distal turbidite or contourite (L6)

The overall compositional trend observed between channel and lobe depositional settings is disturbed by the anomalous composition of L6 (Figs. 5, 14 and 15). However, the apparent similar composition of L6 with the siliciclastic laminae of L5 (L5a) suggests a genetic relationship (Fig. 11F and H).

The turbiditic flow is not sufficient to transport polymineralic grains (*L* and *QFr* grains) which are deposited upstream. The calcareous component (*Fc*, *RA* and *&Bc* grains) from the bioclastic laminae of lithofacies L5b is carried away due to their slower settling velocity, whereas the denser siliciclastic fraction remains in place and accumulates in L6. The very fine sand to silt grain-size distribution and the moderately well sorting (Fig. 5) support a slower settling velocity and a stronger hydrodynamic sorting (Komar, 1985). Such deposit may correspond either to a distal turbidite or to a contourite. However, bioturbation, which is frequently observed in contourites, is missing here and sedimentary features are preserved. Such a lag deposit (Weltje and Prins, 2003) might result from the reworking of fine turbiditic deposits (e.g. L5) by bottom currents (Stanley, 1993; Shanmugam, 2000; Stow et al., 2002). Nonetheless, several fine-grained turbidite deposits were erroneously interpreted as contourites because both deposits share similar characteristic which makes distinctions difficult (Stow et al., 1998, 2002). In most of these cases, Stow et al. (1998) suggest reworking by the tail of the turbiditic flow as a depositional process, and preclude a bottom-current influence. A third explanation might be deposition during lofting (Zavala and Arcuri, 2016). The deposition of the siliciclastic component might trigger lofting, rising up the bioclastic component before its final deposition.

L6 might be considered as an equivalent to the Ölquartzite facies (Tercier, 1947; Trümpy, 1960; Winkler, 1984; Winkler et al., 1985, 1990; Jeanbourquin, 1991) of the Swiss Alpine flyschs. This facies is

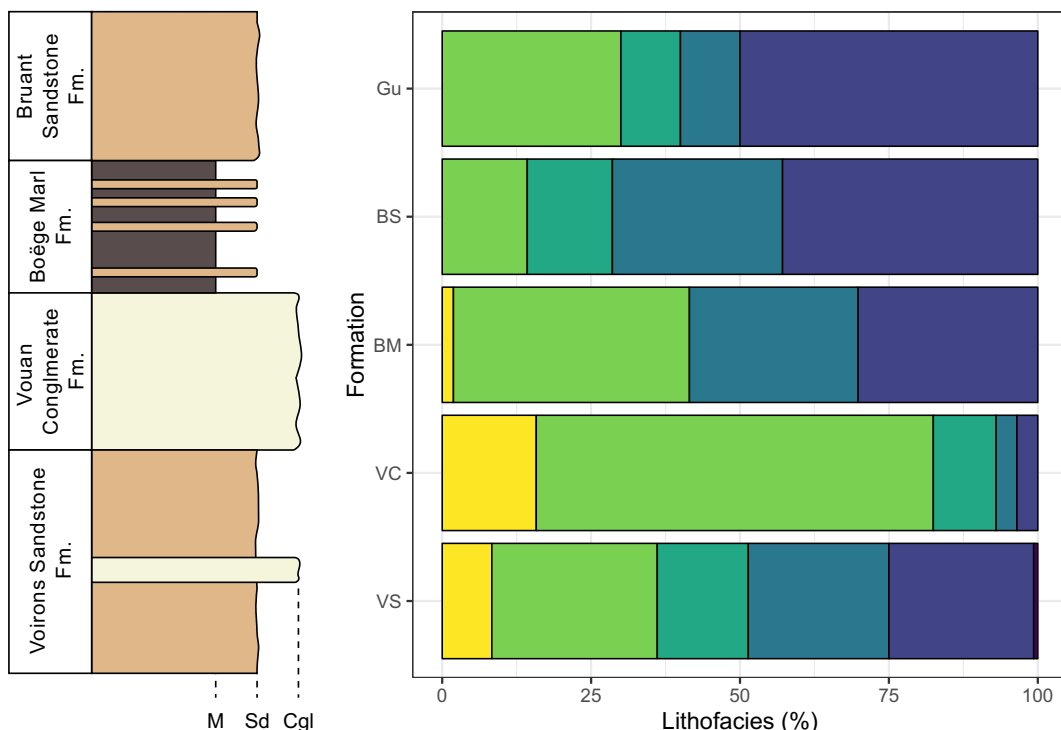


Fig. 17. Relative distribution of the petrofacies within each stratigraphic formation of the Voiron Flysch.

usually associated with the pelagic deposits forming the lowermost part of the succession. Evidence of reworking by bottom currents was suggested due to charcoal lineations within hemipelagic green shales (Hubert, 1967).

This deposit underwent a significant compaction similar to that in channel equivalent (Fig. 7). The important quartzose composition shows abundant pressure dissolution. Furthermore, calcite cement is missing leading to the preservation of the high initial porosity (Fig. 7B). The slow and discontinuous sedimentation of turbiditic flows represents a long time span. In association with the subsequent reworking of the bioclastic fraction, glauconite strongly increases in contrast to the upstream facies (Figs. 14 and 15) and constitutes the second major grain. It is also found filling the porosity of bioclasts (foraminifers and echinoderms) in the upstream facies. The scarcity of feldspars can be explained by the extensive reworking of former distal turbidites (L5a) by bottom currents or a depleted feldspar source (e.g. Quartzose petrofacies). However, such a depletion is also consistent with the negative correlation of feldspar with the mean grain-size (Fig. 6) which contrasts with a preferential dissolution reported in coarser deposits (Milliken, 1992). The association of mature glauconite (yellowish tint) and fresh grains (green tint) indicates different origins (Fig. 11F). This mineral is frequently reworked (Amorosi, 1997) in active tectonic settings and indicates a paraautochthonous source (Amorosi, 1995; Banerjee et al., 2016). The high amount in distal deposits indicates easier transportation than grain-size equivalent detrital grains (Amorosi, 1997). The granular shape indicates long starvation and favourable conditions to replace initial grains (Odin and Matter, 1981).

5.3. Stratigraphy

The large diversity of lithofacies (L1–L6) of the Voirons Sandstone Fm. reflects the variety of its lithologies, also emphasised by the variable amount of marls. L3 to L5 are predominant followed by secondary L1–L2. This confirms the “immature settings” of the initial deposits as suggested by Winkler (1984) for the Voirons-Wägital complex. The prevailing L1 and L2 corroborate the channel interpretation of the Vouan Conglomerate Fm. (Frébourg, 2006; Ospina-Ostios et al., 2013). Surprisingly, the predominantly shaly interval of the Boëge Marl Fm. is mostly represented by transitional stages between channel (L3) and lobe depositional settings (L4). In contrast, end members (L1–L2 and L5) are scarce. The association of fine-grained sediments (Fig. 4C), shaly intervals (Fig. 2G) and intermediate facies (Fig. 17) does not correspond to previous interpretations (Ospina-Ostios et al., 2013) but suggests a modification of the sedimentary flux. The abrupt transition from amalgamated coarse

deposits of channel settings (Vouan Conglomerate Fm.) to the marly dominated interval interspersed by fine sandstone layers (Boëge Marl Fm.), suggests a starved environment, possibly consecutive to a sea-level rise. The low sedimentary input may have weakened the deep-sea fan, and triggered gravity flows from slope-apron instability. The abundant Tb-Td Bouma intervals, the relatively low amount of Ta and the cm-thick sandstone beds, all suggest deposition from surge-like density flows (Mulder and Alexander, 2001). Such an interpretation corroborates the continental-slope settings described by Winkler (1984). The Bruant Sandstone Fm. describes a similar facies distribution than the Voirons Sandstone Fm. However, distal deposits are more frequent. Finally, samples from the other flysch of the Voirons-Wägital complex show a similar distribution than the Voirons Sandstone Fm. and the Bruant Sandstone Fm. However, the small sampling is not relevant to provide a general interpretation for the rest of the nappe.

It is noteworthy that upstream deposits of leveed fan valleys present thick sand accumulation whereas, fans are characterised by thin sand deposits interspersed by marly layers (Lüthi, 1981). In our case study, the lithofacies distribution correlates to the lithostratigraphy of the different stratigraphic units of the Voirons Flysch (Fig. 17). Moreover, the correlation of mean grain size with the successive stratigraphic units of the Voirons Flysch (Fig. 4C) confirms that grain size is also correlated with bed thickness (Sestini, 1970; Gladstone and Sparks, 2002). Thus, lithofacies distribution, emphasised by the compositional variations, is an accurate tool to identify the depositional settings in deep-sea gravity flows.

5.4. Provenance implications

In active tectonic settings, weathering has a limited impact on detrital sediments since sedimentary transport is short with scarce to no intermediate depositional stage (Dickinson and Suczek, 1979; Johnsson, 1993). Detrital sediments entering in a marine basin mostly reflect source-rock lithologies (allogenic factor) and incorporate intrabasinal shelf component (Bc and possibly Lc grains). Then, sediments are carried basinward by gravity flows. Results demonstrate that the hydrodynamic regime of gravity flows (autogenic factor) distributes detritus in a proximal to distal gradient while maintaining an overall similar detrital composition.

The Voirons Flysch is fed by two provenances related to the same palaeogeographic area (Ragusa et al., 2017): the Quartzose and Feldspathic petrofacies. These petrofacies are basically distinguished by the quartz:feldspar ratio. The distribution of samples within each petrofacies shows an elongation toward the L end-member (Fig. 2).

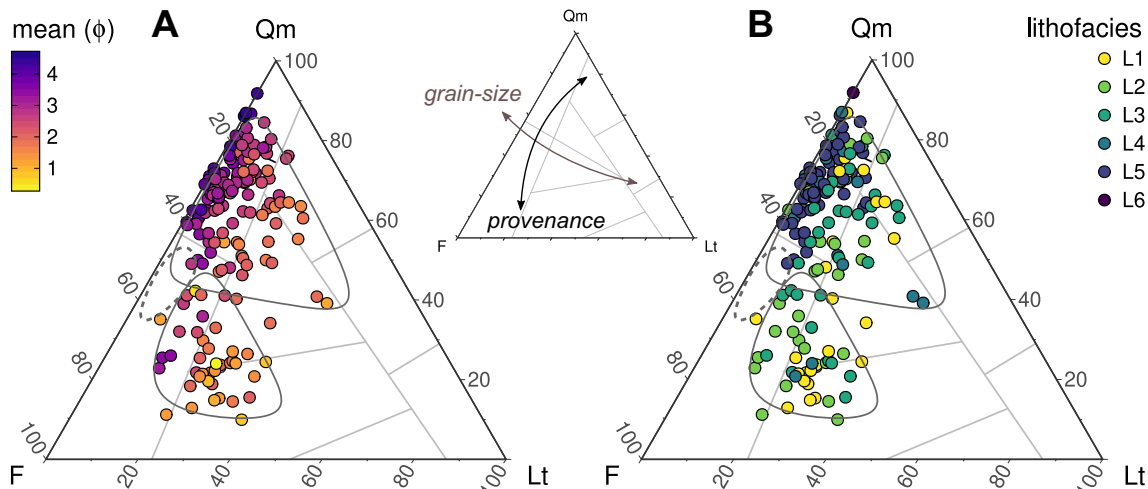


Fig. 18. Distribution of mean grain-size (A) and petrofacies (B) in the QmFlt ternary diagrams referring to Fig. 3. The sample distribution is governed by both provenance and grain-size parameters.

Moreover, the Feldspathic petrofacies describes a more restrictive distribution than the Quartzose petrofacies and lithic-poor samples are rare.

The use of the lithofacies better constrains the sample distribution. Once reported in the QmFlt diagram of the Dickinson model (Dickinson and Suczek, 1979; Dickinson, 1985), the lithofacies are distributed following a similar gradient in both petrofacies (Fig. 18) influence the sample distribution in the provenance model. Hence, channel-related lithofacies (L1–L3) are lithic-rich and thus located in the *Mixed to Recycled Orogens* fields, whereas lithofacies from lobe settings (L4–L5) and reworked depositional settings (L6) are depleted in lithic grains and plot in the *Continental Bloc* field. This trend corroborates similar results from previous analysis of turbiditic deposits in the Apennines (Zuffa, 1985) and from different source-rock lithologies (Ingersoll et al., 1984). However, the different tectonic settings are not relevant with the provenance of the Voiron Flysch.

In our case study, two factors control the sample distribution (Fig. 18). The major one, the provenance (allogenic factor), identified from the quartz:feldspar ratio, distinguishes two major detrital groups (Quartzose and Feldspathic petrofacies) which are organised following the weathering trend of the *Continental Block* domain, whereas the lithofacies (autogenic factor), corresponding to grain-size and depositional settings, defines the sample distribution within each provenance along a channel-lobe axis (or upstream-downstream). Coarse-grained channel deposits lead to a slightly different provenance interpretation than coeval fine-grained lobe sediments (Zuffa, 1985; Fig. 18). Here, grain-support mechanisms and physical properties of grains (density, shape, internal structure) contribute to compositional variations, whereas mechanical break-down has minor effect on sediment types. The lack of clear distinction between the different lithofacies shows that the hydrodynamic behaviour is more complex than the model expects. Furthermore, we cannot exclude petrographic changes across sequence stratigraphy boundary (Dutton and Loucks, 2010; Amorosi and Zuffa, 2011) as neither the whole body geometry nor equivalent platform deposits are known for the Voiron-Wägital complex. The gradual compositional change from proximal to distal settings indicates that the Dickinson model is not relevant to interpret the provenance of deep-sea gravity-flow deposits (Garzanti et al., 2007). Compositional trends are well described in provenance analysis (Dickinson and Suczek, 1979; Dickinson, 1985; von Eynatten, 2004; Garzanti and Andò, 2007). They are generally associated with transitional tectonic settings within a given provenance (e.g. *undissected to dissected Volcanic Arc*) or positioned between two tectonic settings (Mack, 1984). Therefore, the Gazzi-Dickinson method does not remove the grain-size discrimination of the petrofacies distribution in the QmFlt ternary diagram (Ingersoll et al., 1984; Garzanti et al., 2009; Amorosi and Zuffa, 2011). These interpretations confirm distinctions about petrographic composition between channel and lobe settings in deep-sea fans (Fontana et al., 1989; Mansurbeg et al., 2009).

This trend also helps to overcome some limitations related to the scarcity of exposures. The restricted distribution of the Feldspathic petrofacies likely results from the lack of outcrops in distal deposits. However, we can predict the distribution of these missing deposits in the *Basement Uplift* field (Fig. 18, dotted line), by considering a progressive depletion of lithic grains (*L*) in lobe settings. The presence of lobe-related lithofacies within the channel deposits emphasises the complex architecture of the channel system, including levées, overbank deposits and channel migration.

The environmentally controlled compositional variation within both petrofacies suggests that it is important to analyse the whole deep-sea gravity-flow system in order to capture the entire detrital signature. When end-members are missing, compositional variations help to reconstruct the missing values. However, proximal facies are most suitable in source to sink studies. Their lithic-rich composition provides a direct link with the parent-rock assemblages in the source area (Weltje, 2002). However, compaction may affect the preservation of

labilized grains as clayey-silty fragments as well as schistose metamorphic clasts. Inversely, the high amount of intrabasinal grains in lobes deposits is related to autogenic factors, such as the reworking of platform fauna (Ragusa, 2015; Ragusa et al., 2017) in the case of the Voiron Flysch.

In addition, our results show that comparisons between several deep-sea fans can only be made between similar depositional settings. Indeed, comparing the petrography of channel deposits with that of lobe systems will lead to false interpretations (Fig. 18). We have indeed demonstrated how the sedimentary mechanisms and inherited diagenetic processes influence the interpretation of gravity-flow deposits. As Mack (1984) said: "The indiscriminate use of sandstone composition as an indicator of plate-tectonic setting may result in errors in tectonic interpretation." (p. 218).

6. Conclusions

The examination of the grain-size distribution, the sedimentary features and the framework composition of the Voiron Flysch shows the importance of gravity-flow mechanisms on the final composition of these detrital sediments and their subsequent interpretation in the framework of a source to sink analysis.

1. Six lithofacies (L1 to L6) were identified. They display compositional changes along a basinward gradient coupled with a finer grain-size and more distal sedimentary features.
2. The proximal lithofacies (L1 to L3) show a bimodal, poorly sorted, coarse grain-size distribution. Framework grains are dominated by siliciclastic particles. Cement is scarce to missing and porosity reaches up to 30%. Mechanical compaction controls diagenetic processes. We suggest deposition from hyperconcentrated to concentrated density flows.
3. The distal lithofacies (L4 to L5) comprise well-sorted, fine sandstone to coarse siltstone. Early calcite cement fills the intragranular voids. The sedimentary fabric evolves toward a cement-supported framework. Calcareous grains are more frequent and coupled with widespread cement. Distal facies were likely deposited by concentrated density to turbiditic flows.
4. The porous glauconitic quartzarenite (L6) corresponds to reworked distal turbidites or possibly contourites. The well sorted grain-size distribution and constrained framework composition result from further hydraulic reworking of previous deposits by bottom currents.
5. Framework composition, grain-size distribution and Mutti facies are well correlated suggesting a close relationship between the hydrodynamic mechanisms, sedimentary fabrics and the petrography of deep-sea gravity-flow deposits.
6. Possible misinterpretation of tectonic settings from the study of deep-sea gravity-flow deposits is emphasised by the basinward compositional variation identified in the Voiron Flysch: channel deposits are located in the *Mixed* and *Undissected volcanic arc* field, whereas lobe deposits are concentrated in the *Continental block* field.
7. The outcome of this study should be remembered in any future investigation on the provenance of deep-sea, gravity-flow deposits and supports that grain-size distribution greatly influences results of framework composition, heavy mineral population or single-grain studies in provenance analyses.

Acknowledgements

We are grateful to the constructive review and remarks of Kitty Lou Milliken and critical reviews by the editor.

Data availability

Datasets of the modified framework composition and grain-size are available on the GitHub page of the first author (<https://github.com/jragusa/>) and in the electronic supplementary materials.

Funding

This research did not receive any specific grant from funding agencies in the public, commercial, or not-for-profit sectors.

Appendix A. Supplementary data

Supplementary data to this article can be found online at <https://doi.org/10.1016/j.sedgeo.2018.08.010>.

References

- Aitchison, J., 1986. *The Statistical Analysis of Compositional Data*. Chapman and Hall, New York.
- Alboukadel, K., Fabian, M., 2017. Factoextra: Extract and Visualize the Results of Multivariate Data Analyses R package version 1.0.5.
- Amorosi, A., 1995. Glaucony and sequence stratigraphy: a conceptual framework of distribution in siliciclastic sequences. *Journal of Sedimentary Research* 65B, 419–425.
- Amorosi, A., 1997. Detecting compositional, spatial, and temporal attributes of glaucony: a tool for provenance research. *Sedimentary Geology* 109, 135–153.
- Amorosi, A., Zuffa, G.G., 2011. Sand composition changes across key boundaries of siliciclastic and hybrid depositional sequences. *Sedimentary Geology* 236, 153–163.
- dos Anjos, S.M.C., De Ros, L.F., Schiffer de Souza, R., de Assis Silva, C.M., Sombra, C.L., 2000. Depositional and diagenetic controls on the reservoir quality of lower cretaceous Pendéncia sandstones, Potiguar rift basin, Brazil. 84. AAPG Bulletin, pp. 1172–1179.
- Banerjee, S., Bansal, U., Vilas Thorat, A., 2016. A review on palaeogeographic implications and temporal variation in glaucony composition. *Journal of Palaeogeography* 5, 43–71.
- Basu, A., 1976. Petrology of Holocene fluvial sand derived from plutonic source rocks; implications to palaeoclimatic interpretation. *Journal of Sedimentary Research* 46, 694–709.
- Bjorkum, P.A., Walderhaug, O., 1990. Geometrical arrangement of calcite cementation within shallow marine sandstones. *Earth-Science Reviews* 29, 145–161.
- Blatt, H., Middleton, G.V., Murray, R., 1980. *Origin of Sedimentary Rocks*. Prentice Hall.
- Bloch, S., Lander, R.H., 2002. Anomalously high porosity and permeability in deeply buried sandstone reservoirs: Origin and predictability. *AAPG Bulletin* 86, 301–328.
- Bloch, J.D., Timmons, J.M., Crossey, L.J., Gehrels, G.E., Karlstrom, K.E., 2006. Mudstone petrology of the Mesoproterozoic Unkar Group, Grand Canyon, U.S.A.: provenance, weathering, and sediment transport on Intracratonic Rodinia. *Journal of Sedimentary Research* 76, 1106–1119.
- Blott, S.J., Pye, K., 2001. GRADISTAT: a grain size distribution and statistics package for the analysis of unconsolidated sediments. *Earth Surface Processes and Landforms* 26, 1237–1248.
- Bouma, A.H., 1962. *Sedimentology of some Flysch Deposits: A Graphic Approach to Facies Interpretation*. Elsevier, Amsterdam.
- Bouma, A.H., 1972. Fossil contourites in Lower Niesenflysch, Switzerland. *Eclogae Geologicae Helvetiae* 66, 315–323.
- Brownier, J., 1965. Agglutinated foraminifera from some turbiditic sequences. *Proceedings of the Koninklijke Nederlandse Akademie van Wetenschappen, Series A* 68, 309–334.
- Brunner, C.A., Normark, W.R., 1985. Biostratigraphic implications for turbidite depositional processes on the Monterey Deep-Sea Fan, Central California. *Journal of Sedimentary Research* 55, 495–505.
- Burroughs, W.A., 1985. The hydraulic equivalence of Mica: discussion. *Journal of Sedimentary Petrology* 55, 291–294.
- Büttler, E., Winkler, W., Guillong, M., 2011. Laser ablation U/Pb age patterns of detrital zircons in the Schlieren Flysch (Central Switzerland): new evidence on the detrital sources. *Swiss Journal of Geosciences* 104, 225–236.
- Cantalejo, B., Pickering, K.T., 2014. Climate forcing of fine-grained deep-marine systems in an active tectonic setting: Middle Eocene, Ainsa Basin, Spanish Pyrenees. *Palaeogeography, Palaeoclimatology, Palaeoecology* 410, 351–371.
- Caron, C., 1972. La Nappe Supérieure des Préalpes: subdivisions et principaux caractères du sommet de l'édifice préalpin. *Eclogae Geologicae Helvetiae* 65, 57–73.
- Caron, C., 1973. Survol géologique des Alpes occidentales. *Bulletin de la Société Fribourgeoise des Sciences Naturelles* 62, 73–81.
- Caron, C., 1976. La nappe du Gurnigel dans les Préalpes. *Eclogae Geologicae Helvetiae* 69, 297–308.
- Caron, C., Homewood, P., Morel, R., Van Stuijvenberg, J., 1980. Témoins de la Nappe du Gurnigel sur les Préalpes médianes: une confirmation de son origine ultrabriançonnaise. *Bulletin de la Société fribourgeoise des Sciences naturelles* 69, 64–79.
- Caron, C., Homewood, P., Wildi, W., 1989. The original Swiss flysch: a reappraisal of the type deposits in the Swiss prealps. *Earth-Science Reviews* 26, 1–45.
- Cartigny, M.J.B., Ventra, D., Postma, G., van Den Berg, J.H., 2014. Morphodynamics and sedimentary structures of bedforms under supercritical-flow conditions: new insights from flume experiments. *Sedimentology* 61, 712–748.
- Cheel, R.J., 1984. Heavy mineral shadows, a new sedimentary structure formed under upper-flow-regime conditions; its directional and hydraulic significance. *Journal of Sedimentary Research* 54, 1175–1182.
- Crimes, P.T., Goldring, R., Homewood, P., van Stuijvenberg, J., Winkler, W., 1981. Trace fossil assemblages of deep-sea fan deposits, Gurnigel and Schlieren flysch (Cretaceous-Eocene, Switzerland). *Eclogae Geologicae Helvetiae* 74, 953–995.
- Decker, J., Helmold, K.P., 1985. The effect of grain size on detrital modes: a test of the Gazzi-Dickinson point-counting method – discussion. *Journal of Sedimentary Petrology* 55, 618–620.
- Dickinson, W.R.A., 1970. Interpreting detrital modes of graywacke and arkose. *Journal of Sedimentary Petrology* 40, 695–707.
- Dickinson, W.R.A., 1974. Plate tectonics and sedimentation. In: Dickinson, W.R. (Ed.), *Tectonics and Sedimentation*. SEPM Special Publication, Tulsa, OK, pp. 1–27.
- Dickinson, W.R.A., 1985. Interpreting provenance relations from detrital modes of sandstones. In: Zuffa, G.G. (Ed.), *Provenance of Arenites*. NATO ASI - Series C: Mathematical and Physics Sciences. D. Reidel Publishing Company, Dordrecht, pp. 333–361.
- Dickinson, W.R.A., Suczek, C., 1979. Plate tectonics and sandstone compositions. *AAPG Bulletin* 63, 2164–2182.
- Dickson, J.A.D., 1965. A modified staining technique for carbonates in thin section. *Nature* 205, 587.
- Dickson, J.A.D., 1966. Carbonate identification and genesis as revealed by staining. *Journal of Sedimentary Research* 36, 491–505.
- Dott, R.H., 1964. Wacke, Graywacke and matrix—what approach to immature sandstone classification? *Journal of Sedimentary Research* 34, 625–632.
- Doyle, L.J., Carder, K.L., Steward, R.G., 1983. The hydraulic equivalence of Mica. *Journal of Sedimentary Research* 53, 643–648.
- Doyle, L.J., Carder, K.L., Steward, R.G., 1985. The hydraulic equivalence of Mica: reply. *Journal of Sedimentary Petrology* 55, 293–294.
- Dutton, S., Loucks, R., 2010. Diagenetic controls on evolution of porosity and permeability in lower Tertiary Wilcox sandstones from shallow to ultradeep (200–6700m) burial, Gulf of Mexico Basin, U.S.A. *Marine and Petroleum Geology* 27, 1775–1787.
- von Eynatten, H., 2004. Statistical modelling of compositional trends in sediments. *Sedimentary Geology* 171, 79–89.
- Folk, R.L., 1980. *Petrology of Sedimentary Rocks*. Hemphill Publishing Company, Austin.
- Fontana, D., Zuffa, G.G., Garzanti, E., 1989. The interaction of eustacy and tectonism from provenance studies of the Eocene Hecho Group Turbidite Complex (South-Central Pyrenees, Spain). *Basin Research* 2, 223–237.
- Frébourg, G., 2006. Les Conglomérats du Vouan: un cañon turbiditique?. (PhD thesis). University Of Geneva.
- Friedman, G.M., 1958. Determination of sieve-size distribution from thin-section data for sedimentary petrological studies. *The Journal of Geology* 66, 394–416.
- Friedman, G.M., 1962. Comparison of moment measures for sieving and thin-section data in sedimentary petrological studies. *Journal of Sedimentary Petrology* 32, 15–25.
- Friedman, G.M., 1996. Thin section grain size analysis revisited: discussion. *Sedimentology* 43, 189.
- Garzanti, E., 1986. Source rock versus sedimentary control on the mineralogy of deltaic volcanic arenites (Upper Triassic, Northern Italy). *Journal of Sedimentary Research* 56, 267–275.
- Garzanti, E., Andò, S., 2007. Plate tectonics and heavy-mineral suites of modern sands. In: Mange, M.A., Wright, D.T. (Eds.), *Heavy Minerals in Use. Developments in Sedimentology*. Elsevier, Amsterdam, pp. 741–763.
- Garzanti, E., Doglioni, C., Vezzoli, G., Andò, S., 2007. Orogenic belts and orogenic sediment provenance. *The Journal of Geology* 115, 315–334.
- Garzanti, E., Andò, S., Vezzoli, G., 2008. Settling equivalence of detrital minerals and grain-size dependence of sediment composition. *Earth and Planetary Science Letters* 273, 138–151.
- Garzanti, E., Andò, S., Vezzoli, G., 2009. Grain-size dependence of sediment composition and environmental bias in provenance studies. *Earth and Planetary Science Letters* 277, 422–432.
- Garzanti, E., Resentini, A., Andò, S., Vezzoli, G., Pereira, A., Vermeesch, P., 2015. Physical controls on sand composition and relative durability of detrital minerals during ultra-long distance littoral and aeolian transport (Namibia and southern Angola). *Sedimentology* 62, 971–996.
- Gazzi, P., 1966. Le Arenarie del Flysch Sopraccetaceo dell'Appennino Modenese: Correlazioni con il Flysch di Monghidoro. *Mineralogica et Petrographica Acta* 12, 69–97.
- Gazzi, P., Zuffa, G.G., Gandolfi, G., Paganelli, L., 1973. Provenienza e dispersione littoranea delle sabbie delle spiagge Adriatiche fra le foci dell'Isone e del Fogla: Inquadramento regionale. *Memorie della Società Geologica Italiana* 12, 1–37.
- Gladstone, C., Sparks, R.S.J., 2002. The significance of grain-size breaks in turbidites and pyroclastic current deposits. *Journal of Sedimentary Research* 72, 182–191.
- González-Acebrón, L., Arribas, J., Mas, R., 2010. Role of sandstone provenance in the diagenetic albitization of feldspars. *Sedimentary Geology* 229, 53–63.
- Grantham, J.H., Velbel, M.A., 1988. The influence of climate and topography on rock-fragment abundance in modern fluvial sands of the southern Blue Ridge Mountains, North Carolina. *Journal of Sedimentary Petrology* 58, 219–227.
- Griffiths, J.C., 1967. *Scientific Method in Analysis of Sediments. International Series in the Earth and Planetary Sciences*. McGraw-Hill, New York.
- Hamilton, N., 2017. ggtern: An Extension to "ggplot2", for the creation of Ternary Diagrams. R package version 2.2.1.
- Handy, M.R., Schmid, S.M., Bousquet, R., Kissling, E., Bernoulli, D., 2010. Reconciling plate-tectonic reconstructions of Alpine Tethys with the geological-geophysical record of spreading and subduction in the Alps. *Earth-Science Reviews* 102, 121–158.
- Hesse, R., Butt, A., 1976. Paleobathymetry of Cretaceous Turbidite Basins of the East Alps relative to the calcite compensation level. *The Journal of Geology* 84, 505–533.
- Holmes, M.A., Breza, J., Wise, S., 1987. Provenance and deposition of Lower Cretaceous Turbidite Sands at Deep Sea Drilling Project Site 603, Lower Continental Rise off North Carolina. *Initial Reports of the Deep Sea Drilling Project* 93, 941–960.

- Hsü, J.K., 1964. Cross-laminations in graded bed sequences. *Journal of Sedimentary Research* 34, 379–388.
- Hubert, J.F., 1967. Sedimentology of Prealpine Flysch Sequences, Switzerland. *Journal of Sedimentary Research* 37, 885–907.
- Ingersoll, R.V., Bullard, T.F., Ford, R.L., Grimm, J.P., Pickle, J.D., Sares, S.W., 1984. The effect of grain size on detrital modes: a test of the Gazzi-Dickinson point-counting method. *Journal of Sedimentary Research* 54, 103–116.
- Ingersoll, R.V., Bullard, T.F., Ford, R.D., Pickle, J.D., 1985a. The effect of grain size on detrital modes; a test of the Gazzi-Dickinson point-counting method – reply to discussion of John Decker and Kenneth P. Helmold. *Journal of Sedimentary Petrology* 55, 620–621.
- Ingersoll, R.V., Bullard, T.F., Ford, R.D., Pickle, J.D., 1985b. The effect of grain size on detrital modes; a test of the Gazzi-Dickinson point-counting method – reply to discussion of Lee J. Suttner and Abhijit Basu. *Journal of Sedimentary Petrology* 55, 617–618.
- Jan du Chêne, R., Gorin, G., van Stuijvenberg, J., 1975. Etude géologique et stratigraphique (palyntologie et nannoflore calcaire) des Grès des Voirons (Paléogène de Haute-Savoie, France). *Géologie Alpine* 51, 51–78.
- Jeanbourquin, P., 1991. L'Ultrahelvétique* de Derborence, (Valais, Suisse). *Bulletin de la Murithienne* 109, 65–95.
- Johnson, M.R., 1994. Thin section grain size analysis revisited. *Sedimentology* 41, 985–999.
- Johnson, M.R., 1996. Thin section grain size analysis revisited: reply. *Sedimentology* 43, 190–191.
- Johnsson, M.J., 1993. The system controlling the composition of clastic sediments. In: Johnsson, M.J., Basu, A. (Eds.), *Processes controlling the composition of clastic sediments*. Geological Society of America Special Paper, Boulder, CO, pp. 1–20.
- Jorry, S.J., Hasler, C.-A., Davaud, E., 2006. Hydrodynamic behaviour of Nummulites: implications for depositional models. *Facies* 52, 221–235.
- Kairo, S., Suttner, L.J., Dutta, P.K., 1993. Variability in sandstone composition as a function of depositional environment in coarse-grained delta systems. In: Johnsson, M.J., Basu, A. (Eds.), *Processes Controlling the Composition of Clastic Sediments*. Geological Society of America Special Paper, Boulder, CO, pp. 263–284.
- Kerrien, Y., Turrel, C., Monjuvent, G., Charollais, J., Lombard, A., Balmer, F., Olmari, F., Papillon, R., Fontannaz, L., Amberger, G., Ruchat, C., Grebert, Y., Marthaler, M., 1998. Feuille Annemasse (654) de la Carte géologique de la France (1/50000ème). BRGM, Orléans.
- Kim, J.C., Lee, Y.I., Hisada, K., 2007. Depositional and compositional controls on sandstone diagenesis, the Totori Group (Middle Jurassic–Early Cretaceous), central Japan. *Sedimentary Geology* 195, 183–202.
- Kiminami, K., Fujii, K., 2007. The relationship between major element concentration and grain size within sandstones from four turbidite sequences in Japan. *Sedimentary Geology* 195, 203–215.
- Komar, P.D., 1985. The hydraulic interpretation of turbidites from their grain sizes and sedimentary structures. *Sedimentology* 32, 395–407.
- Komar, P.D., 2007. The entrainment, transport and sorting of heavy minerals by waves and currents. In: Mange, M.A., Wright, D.T. (Eds.), *Heavy Minerals in Use. Developments in Sedimentology*. Elsevier, Amsterdam, pp. 3–48.
- Komar, P.D., Baba, J., Cui, B., 1984. Grain-size analyses of Mica within sediments and the hydraulic equivalence of Mica and Quartz. *Journal of Sedimentary Research* 54, 1379–1391.
- Korsch, R., Roser, B., Kamprad, J., 1993. Geochemical, petrographic and grain-size variations within single turbidite beds. *Sedimentary Geology* 83, 15–35.
- Krynnine, P.D., 1943. Diastrophism and the evolution of sedimentary rocks. *Tulsa Geological Society Digest* 11, 64–65.
- Kuenen, P.H., 1968. Turbidity currents and organisms. *Eclogae Geologicae Helveticae* 61, 525–544.
- Kuenen, P.H., Carozzi, A.V., 1953. Turbidity currents and sliding in Geosynclinal Basins of the Alps. *The Journal of Geology* 61, 363–373.
- Kuenen, P.H., Migliorini, C.J., 1950. Turbidity currents as a cause of graded bedding. *The Journal of Geology* 58, 91–127.
- Lawrence, R.L., Cox, R., Mapes, R.W., Coleman, D.S., 2011. Hydrodynamic fractionation of zircon age populations. *Geological Society of America Bulletin* 123, 295–305.
- Lombard, A., 1940. Géologie des Voirons. Mémoire de la Société helvétique des Sciences Naturelles, Zurich.
- Lowe, D.R., 1982. Sediment gravity flows: II depositional models with special reference to the deposits of high-density turbidity currents. *Journal of Sedimentary Research* 52, 279–297.
- Lundegard, P.D., 1992. Sandstone porosity loss; a “big picture” view of the importance of compaction. *Journal of Sedimentary Research* 62, 250–260.
- Lüthi, S., 1981. Experiments on non-channelized turbidity currents and their deposits. *Marine Geology* 40, M59–M68.
- Mack, G.H., 1984. Exceptions to the relationship between plate tectonics and sandstone composition. *Journal of Sedimentary Research* 54, 212–220.
- Mansurbeg, H., Caja, M., Marfil, R., Morad, S., Remacha, E., García, D., Martín-Crespo, T., El-Ghali, M., Nystuen, J., 2009. Diagenetic evolution and porosity destruction of turbiditic hybrid arenites and siliciclastic sandstones of foreland basins: evidence from the Eocene Hecho Group, Pyrenees, Spain. *Journal of Sedimentary Research* 79, 711–735.
- Martín-Fernández, J.A., Barceló-Vidal, C., Pawlowsky-Glahn, V., 2003. Dealing with zeros and missing values in compositional data sets using nonparametric imputation. *Mathematical Geology* 35, 253–278.
- McBride, E.F., Milliken, K., Cavazza, W., Cibin, U., Fontana, D., Picard, M.D., Zuffa, G.G., 1995. Heterogeneous distribution of calcite cement at the outcrop scale in Tertiary sandstones, Northern Apennines, Italy. *AAPG Bulletin* 79, 1044–1063.
- McLennan, S.M., McCulloch, M.T., Taylor, S.R., Maynard, J.B., 1989. Effects of sedimentary sorting on neodymium isotopes in deep-sea turbidites. *Nature* 337, 547–549.
- Milliken, K.L., 1988. Loss of provenance information through subsurface diagenesis in Plio-Pleistocene sandstones, northern Gulf of Mexico. *Journal of Sedimentary Petrology* 58, 992–1002.
- Milliken, K.L., 1992. Chemical behavior of detrital feldspars in mudrocks versus sandstones, Frio Formation (Oligocene), South Texas. *Journal of Sedimentary Petrology* 62, 790–801.
- Milliken, K.L., 2001. Diagenetic heterogeneity in sandstone at the outcrop scale, Breathitt Formation (Pennsylvanian), eastern Kentucky. *AAPG Bulletin* 85, 795–815.
- Misko, R.M., Hendry, H.E., 1979. The petrology of sands in the uppermost Cretaceous and Palaeocene of southern Saskatchewan: a study of composition influenced by grain size, source area, and tectonics. *Canadian Journal of Earth Sciences* 16, 38–49.
- Moares, M.A.S., Surdam, R.C., 1993. Diagenetic heterogeneity and reservoir quality; fluvial, deltaic, and turbiditic sandstone reservoirs, Potiguar and Reconcavo rift basins, Brazil. *AAPG Bulletin* 77, 1142–1158.
- Morad, S., Bergan, M., Knarud, R., Nystuen, J.P., 1990. Albition of detrital plagioclase in triassic reservoir sandstones from the Snorre Field, Norwegian North Sea. *Journal of Sedimentary Research* 60, 411–425.
- Morad, S., Ketter, J.M., De Ros, L.F., 2000. Spatial and temporal distribution of diagenetic alterations in siliciclastic rocks: implications for mass transfer in sedimentary basins. *Sedimentology* 47, 95–120.
- Morton, A.C., Hallsworth, C.R., 1994. Identifying provenance-specific features of detrital heavy mineral assemblages in sandstones. *Sedimentary Geology* 90, 241–256.
- Morton, A.C., Hallsworth, C.R., 1999. Processes controlling the composition of heavy mineral assemblages in sandstones. *Sedimentary Geology* 124, 3–29.
- Mosar, J., 1991. Géologie structurale dans les Préalpes Médianes (Suisse). *Eclogae Geologicae Helvetiae* 84, 689–725.
- Mu, N., Fu, Y., Schulz, H.-M., van Berk, W., 2016. Authigenic albite formation due to water-rock interactions – case study: Magnus oilfield (UK, Northern North Sea). *Sedimentary Geology* 331, 30–41.
- Mulder, T., Alexander, J., 2001. The physical character of subaqueous sedimentary density flows and their deposits. *Sedimentology* 48, 269–299.
- Mutti, E., 1972. Le torbidi dell'Appennino Settentrionale : introduzione all'anilisi di facies. *Memorie della Società Geologica Italiana* 11, 161–199.
- Mutti, E., 1992. Turbidite Sandstones. Agip, Milano.
- Norman, T.N., 1969. A method to study the distribution of heavy-mineral grain abundance in a turbidite. *Sedimentology* 13, 263–280.
- Odin, G.S., Matter, A., 1981. De glauconiarum origine. *Sedimentology* 28, 611–641.
- Odom, I., 1975. Feldspar–grain size relations in Cambrian Arenites, Upper Mississippi Valley. *Journal of Sedimentary Research* 45, 636–650.
- Oehmig, R., 1993. Entrainment of planktonic foraminifera: effect of bulk density. *Sedimentology* 40, 869–877.
- Ospina-Ostios, L.M., Ragusa, J., Wernli, R., Kindler, P., 2013. Planktonic foraminifer biostratigraphy as a tool in constraining the timing of flysch deposition: Gurnigel flysch, Voirons massif (Haute-Savoie, France). *Sedimentology* 60, 225–238.
- Ospina-Ostios, L.M., 2017. Biostratigraphy and structure of the Voirons Flysch (Gurnigel Nappe, Haute-Savoie, France). PhD thesis, University of Geneva.
- Paxton, S.T., Szabo, J.O., Ajdukiewicz, J.M., Klimentidis, R.E., 2002. Construction of an intergranular volume compaction curve for evaluating and predicting compaction and porosity loss in rigid-grain sandstone reservoirs. *AAPG Bulletin* 86, 2047–2067.
- Piper, D.J.W., 1978. Turbidite muds and silts on deep sea fans and abyssal plains. In: Stanley, D.J., Kelling, G. (Eds.), *Sedimentation in Submarine Canyons, Fans and Trenches*. Hutchinson and Ross, Stroudsburg, PA, pp. 163–176.
- Postma, G., Nemec, W., Kleinspehn, K.L., 1988. Large floating clasts in turbidites: a mechanism for their emplacement. *Sedimentary Geology* 58, 47–61.
- Postma, G., Cartigny, M.J.B., Kleverlaan, K., 2009. Structureless, coarse-tail graded Bouma Ta formed by internal hydraulic jump of the turbidity current? *Sedimentary Geology* 219, 1–6.
- Pyles, D.R., Straub, K.M., Stammer, J.G., 2013. Spatial variations in the composition of turbidites due to hydrodynamic fractionation. *Geophysical Research Letters* 40, 3919–3923.
- R Core Team, 2018. R: A Language and Environment for Statistical Computing, Vienna.
- Ragusa, J., 2015. Pétrographie, stratigraphie et provenance du Flysch des Voirons (Nappe du Gurnigel, Haute-Savoie, France). (PhD thesis). University of Geneva.
- Ragusa, J., Segvic, B., Ospina-Ostios, L.M., Kindler, P., 2017. Provenance analysis of the Voirons Flysch (Gurnigel nappe, Haute-Savoie, France): Stratigraphic and paleogeographic implications. *International Journal of Earth Sciences* 106, 2619–2651.
- Ragusa, J., Ospina-Ostios, L.M., Spezzaferri, S., Kindler, P., 2018. Revision of the planktonic foraminiferal biostratigraphy of the Voirons Flysch (Chablais Prealps, Haute-Savoie, France). *Swiss Journal of Geosciences* 111, 433–445.
- Reed, J.S., Eriksson, K.A., Kowalewski, M., 2005. Climatic, depositional and burial controls on diagenesis of Appalachian Carboniferous sandstones: qualitative and quantitative methods. *Sedimentary Geology* 176, 225–246.
- Ricci-Lucchi, F., 1975. Depositional cycles in two turbidite formations of northern Apennines. *Journal of Sedimentary Research* 45, 3–43.
- Rubey, W.W., 1933. The size-distribution of heavy minerals within a water-laid sandstone. *Journal of Sedimentary Research* 3, 3–29.
- Schmid, S.M., Pfiffner, A.O., Froitzheim, N., Schönborn, G., Kissling, E., 1996. Geophysical-geological transect and tectonic evolution of the Swiss-Italian Alps. *Tectonics* 15, 1036–1064.
- Scholle, P.A., 1971. Sedimentology of fine-grained deep-water carbonate turbidites, Monte Antola Flysch (Upper Cretaceous), Northern Apennines, Italy. *Geological Society of America Bulletin* 82, 629–658.
- Sestini, G., 1970. Flysch facies and turbidite sedimentology. *Sedimentary Geology* 4, 559–597.

- Shanmugam, G., 2000. 50 years of the turbidite paradigm (1950s–1990s): deep-water processes and facies models – a critical perspective. *Marine and Petroleum Geology* 17, 285–342.
- Shideler, G.L., Slaczka, A., Unrug, R., Wendorff, M., 1975. Textural and mineralogical sorting relationships in Krosno Formation (Oligocene) Turbidites, Polish Carpathian Mountains. *Journal of Sedimentary Research* 45, 44–56.
- Spencer, D.W., 1963. The interpretation of grain size distribution curves of clastic sediments. *Journal of Sedimentary Research* 33, 180–190.
- Stanley, D.J., 1963. Vertical petrographic variability in Annot Sandstone Turbidites: some preliminary observations and generalizations. *Journal of Sedimentary Research* 33, 783–788.
- Stanley, D.J., 1993. Model for turbidite-to-contourite continuum and multiple process transport in deep marine settings: examples in the rock record. *Sedimentary Geology* 82, 241–255.
- Stevenson, C.J., Talling, P.J., Mason, D.G., Sumner, E.J., Frenz, M., Wynn, R.B., 2014. The spatial and temporal distribution of grain-size breaks in turbidites. *Sedimentology* 61, 1120–1156.
- Stow, D.A.V., Bowen, A.J., 1980. A physical model for the transport and sorting of fine-grained sediment by turbidity currents. *Sedimentology* 27, 31–46.
- Stow, D.A.V., Mayall, M., 2000. Deep-water sedimentary systems: new models for the 21st century. *Marine and Petroleum Geology* 17, 125–135.
- Stow, D.A.V., Shanmugam, G., 1980. Sequence of structures in fine-grained turbidites: comparison of recent deep-sea and ancient flysch sediments. *Sedimentary Geology* 25, 23–42.
- Stow, D.A.V., Faugères, J.-C., Viana, A.R., Gonthier, E., 1998. Fossil contourites: a critical review. *Sedimentary Geology* 115, 3–31.
- Stow, D.A.V., Faugères, J.-C., Howe, J.A., Pudsey, C.J., Viana, A.R., 2002. Bottom currents, contourites and deep-sea sediment drifts: current state-of-the-art. *Memoirs of the Geological Society* 22, 7–20.
- Studer, B., 1827. Remarques géognostiques sur quelques parties de la chaîne septentrionale des Alpes. *Annales de la Société d'Histoire Naturelle de Paris* 1, 5–47.
- Suttner, L.J., 1974. Sedimentary petrographic province: an evaluation. *Paleogeographic Provinces and Provinciality*, SEPM Special Publication 22 pp. 75–84.
- Suttner, L.J., Basu, A., 1985. The effect of grain size on detrital modes: a test of the Gazzi-Dickinson point-counting method – discussion. *Journal of Sedimentary Petrology* 55, 616–617.
- Suttner, L.J., Basu, A., Mack, G.H., 1981. Climate and the origin of quartz arenites. *Journal of Sedimentary Research* 51, 1235–1246.
- SwissTopo (2008) Carte géologique et tectonique de la Suisse au 1:500'000. SwissTopo, Bern.
- Tercier, J., 1947. Le Flysch dans la sédimentation alpine. *Eclogae Geologicae Helvetiae* 40, 164–198.
- Tolosana-Delgado, R., von Eynatten, H., 2009. Grain-size control on petrographic composition of sediments: compositional regression and rounded zeros. *Mathematical Geosciences* 41, 869–886.
- Tomkins, M.R., Nielsen, P., Hughes, M.G., 2003. Selective entrainment of sediment graded by size and density under waves. *Journal of Sedimentary Research* 73, 906–911.
- Trask, C.B., Hand, B.M., 1985. Differential transport of fall-equivalent sand grains, Lake Ontario, New York. *Journal of Sedimentary Research* 55, 226–234.
- Trümpy, R., 1960. Paleotectonic evolution of the central and western Alps. *Geological Society of America Bulletin* 71, 843–908.
- Trümpy, R., 2006. Geologie der Iberger Klippen und ihrer Flysch-Unterlage. *Eclogae Geologicae Helvetiae* 99, 79–121.
- Ujetz, B., 1996. Micropaleontology of Paleogene deep water sediments, Haute-Savoie, France. (PhD thesis), University of Geneva.
- Van Stuijvenberg, J., 1980. Stratigraphie et structure de la Nappe du Gurnigel aux Voiron, Haute-Savoie. *Bulletin de la Société fribourgeoise des Sciences naturelles* 69, 80–96.
- Van Stuijvenberg, J., Morel, R., Jan Du Chêne, R., 1976. Contribution à l'étude des flyschs de la région de Fayaux (Préalpes externes vaudoises). *Eclogae Geologicae Helvetiae* 69, 309–326.
- Walker, R.G., 1973. Mopping-up the turbidite mess. A history of the turbidity current concept. In: Ginsburg, R.N. (Ed.), *Evolving Concepts in Sedimentology*. John Hopkins University Press, Baltimore, MD, pp. 1–37.
- Weidmann, M., 1967. Petite contribution à la connaissance du flysch. *Bulletin de la Société Vaudoise des Sciences Naturelles* 69, 395–400.
- Weltje, G.J., 2002. Quantitative analysis of detrital modes: statistically rigorous confidence regions in ternary diagrams and their use in sedimentary petrology. *Earth-Science Reviews* 57, 211–253.
- Weltje, G.J., Prins, M.A., 2003. Muddled or mixed? Inferring palaeoclimate from size distributions of deep-sea clastics. *Sedimentary Geology* 162, 39–62.
- Wentworth, C.K., 1922. A scale of grade and class terms for clastic sediments. *The Journal of Geology* 30, 377–392.
- Winkler, W., 1983. Stratigraphie, Sedimentologie und Sediment-petrographie des Schlieren-Flysches (Zentralschweiz). *Matériaux pour la Carte Géologique Suisse. Société Helvétique des Sciences Naturelles*, Bern.
- Winkler, W., 1984. Palaeocurrents and petrography of the Gurnigel-Schlieren flysch: a basin analysis. *Sedimentary Geology* 40, 169–189.
- Winkler, W., Wildi, W., Van Stuijvenberg, J., Caron, C., 1985. Wägital-Flysch et autres flyschs pennique en Suisse Centrale. *Stratigraphie, sédimentologie et comparaisons. Eclogae Geologicae Helvetiae* 78, 1–22.
- Winkler, W., Hurford, A.J., von Salis Perch-Nielsen, K., Odin, G.S., 1990. Fission track and nannofossil ages from a Palaeocene bentonite in the Schlieren Flysch (Central Alps, Switzerland). *Schweizerische mineralogische und petrographische Mitteilungen* 70, 389–396.
- Wissing, S.B., Pfiffner, A.O., 2002. Structure of the eastern Klippen nappe (BE, FR): implications for its Alpine tectonic evolution. *Eclogae Geologicae Helvetiae* 95, 381–398.
- Yang, S., Zhang, F., Wang, Z., 2012. Grain size distribution and age population of detrital zircons from the Changjiang (Yangtze) River system, China. *Chemical Geology* 296–297, 26–38.
- Zavala, C., Arcuri, M., 2016. Intrabasinal and extrabasinal turbidites: origin and distinctive characteristics. *Sedimentary Geology* 337, 36–54.
- Zimmerle, W., 1973. Fossil heavy mineral concentrations. *Geologische Rundschau* 62, 536–548.
- Zuffa, G.G., 1985. Optical analyses of arenites: influence of methodology on compositional results. In: Zuffa, G.G. (Ed.), *Provenance of Arenites*. NATO ASI Series. Springer Netherlands, Dordrecht, pp. 165–189.
- Zuffa, G.G., 1987. Unravelling Hinterland and Offshore Palaeogeography from deep-water arenites. In: Leggett, J.K., Zuffa, G.G. (Eds.), *Marine Clastic Sedimentology*. Springer Netherlands, Dordrecht, pp. 39–61.
- Zuffa, G.G., 1991. On the use of turbidite arenites in provenance studies: critical remarks. *The Geological Society, Special Publications* 57 pp. 23–29.